CAAP Quarterly Report

Date of Report: 12/27/2022

Prepared for: U.S. DOT Pipeline and Hazardous Materials Safety Administration

Contract Number: 693JK32250009CAAP

Project Title: "All-in-One Multifunctional Cured-In-Place Structural Liner for Rehabilitating of Aging Cast Iron Pipelines"

Prepared by: Ying Huang (PI), Long Jiang, Zhibin Lin, Chengcheng Tao, and Liangliang Huang

Contact Information: Ying Huang, Email: ying.huang@ndsu.edu, Phone: 701.231.7651

For quarterly period ending: 12/27/2022

Business and Activity Section

(a) Contract Activity

Discussion about contract modifications or proposed modifications:

None.

Discussion about materials purchased:

Steel plate coupons, epoxy, carbon nanotubes.

(b) Status Update of Past Quarter Activities

In this quarter, the university research team completed Task 1 of this project, including a kick-off meeting with PHMSA program managers on Nov. 22nd, 2022 and a thorough literature review on related topics, in addition to hiring six graduate students and one undergraduate student for the project and an outreach event to middle school students as “Pipeline Challenge” in BrainSTEM on Oct. 25th, 2022 to expand the educational impact of this project.

(c) Cost share activity

None.

(d) Task 1: Kick-off meeting and literature review

In this task, four activities were performed, including (1) a kick-off meeting with PHMSA personnel held on Nov. 22nd, 2022 to ensure that the project objectives and tasks follow the DOT and PHMSA’s expectations and guidelines; (2) a thorough literature review performed on related topics of the proposed research, which included but not limited to the pipeline liners, recent developments of vitrimers and their applications in self-healing, high-performance epoxy materials, assessment and monitoring of liners, finite element modeling of pipelines and liners, and risk analysis of pipelines and liners; (3) hiring six graduate students and one undergraduate researcher to work on this project; and (4) an outreach event conducted to middle school students on Oct. 25th, 2022 as “Pipeline Challenge” outreach project.

1. Background and Objectives in the 1th Quarter

1.1 Background

This project is designed to develop and test the feasibility of an all-in-one multifunctional Cured-In-Place Pipe (CIPP) structural liner that is self-healing and self-sensing with high performance. Specifically, the all-in-one CIPP structural liner has the following innovations to achieve the multifunction: 1) the healing capacity is enabled by using the solvent-free and catalyst-free vitrimer epoxy/anhydride and/or epoxy/acid resins for recyclable, sustainable, and environmental friendly liner applications; 2) the high performance is achieved by modifying the epoxy resin using surface treated nanofillers (e.g. carbon nanotubes) and guided by molecular dynamics simulation and computational finite element analysis to enhance the liner's mechanical and bonding properties and reduce the permeability; and 3) the self-sensing function is supported by embedding distributed fiber optic sensors along with the fabric of the liner to monitor its health condition during installation and service, such as damages, debond, cracks, etc., and by integrating with the artificial intelligence to develop a CIPP liner risk index for risk assessment and integrity management. Upon validation, the multifunction of such an all-in-one CIPP structural liner can be partially or fully implemented with commercially available CIPP solutions to enhance the sustainability and reliability of CIPP technologies in practice for better mitigating risks of the repaired aging cast iron pipelines. In the first quarter of this project, literature review was expected to direct the research to the right direction for the development of the all-in-one liner in future quarters.

1.2 Objectives in the 1th Quarter

In the first quarter, the major objective is to effectively communicate with PHMSA personnel to understand the specific requirements. More specifically, there are two sub-objectives as aligned in the proposal:

(1) Kick-off meeting with PHMSA personnel to ensure that the project objectives and tasks follow the DOT and PHMSA's expectations and guidelines;

(2) Literature review on related topics of the proposed research.

2. Results and Discussions

2.1 Kick-off Meeting

On Nov. 22rd, 2022 (1:30 -3:00 pm CT), a zoom kick-off meeting was conducted between the PHMSA program managers, the advisory board member, and the research team. All PIs attended the kick-off meeting. A web presentation was made to the PHMSA personnel followed by questions/answers and discussions.

2.2 Literature Review

The detailed reviews on the pipeline liners, recent developments of vitrimers and their applications in self-healing, high-performance epoxy materials, chemical analysis of surface bonding and permeability, assessment and monitoring of liners, finite element modeling of pipelines and liners, and risk analysis of pipelines and liners. A total of 134 literatures have been reviewed and summarized in the review detailed below.

2.2.1 CIIP Pipeline Liner

Currently, the United States still has 26,060 miles of cast iron pipelines in service. These cast iron pipelines mostly have a service period of more than a hundred year. With aging and corrosion, some of them may leak or crack and need to be repaired, rehabilitated, or even replaced. Replacing leaking pipeline segments using open-trench approach is the most common practice. However, it may not be feasible to replace the pipeline segments using open-trench method in some circumstances, such as when the pipelines are in highly populated areas, in areas with congested pipeline systems and do not have sufficient right-of-way space for open trench, or in areas where it is not cost-effective for excavation and restoration costs. In these circumstances, trenchless technologies became a potential alternative to rehabilitate the aging cast-iron pipelines[1]. There are two major trenchless technologies to rehabilitate oil and natural gas production applications, including the composite pipes and the CIPP structural liners. The commercially available composite pipes include the primus line[2], the high-density polyethylene smart pipe[3], FlexSteel pipe, Fiberspar LinePipe[4], the Polyflow Thermoflex Tubing, and the Flexpipe system. Many of the composite pipes are spoolable pipes manufactured in various sizes and in continuous lengths up to 35,000 ft for pipes of small diameters. These composite pipes usually have an internal thermoplastic liner surrounded by laminates made of carbon, glass, or other fibers in an epoxy resin base as the pressure-carrying components of the composite. The use of those different materials allows for high pressure ratings for those pipes to be utilized for transmission lines. Although the applications of composite pipes can bear high pressures, the expensive cost and the small diameter features have limited their wide applications[1].

To seek more affordable and flexible trenchless alternatives for preventing pipeline leakage and increasing the service life of cast-iron pipelines, the CIPP liner has evolved into a well-accepted technology in practice [1, 5, 6]. Worldwide, it is estimated that nearly 75,000 miles of pipelines, including natural gas pipes, water and wastewater pipes, have been rehabilitated with CIPP liners, with nearly $3 billion spent annually on the trenchless renovation method. The CIPP liner (e.g. Starline HPL-G29) is a hollow cylinder containing a non-woven or woven fabric material impregnated by a cured thermosetting resin. The resin is impregnated into the fabric in a factory and prefabricated and transported to sites. Then, the liner is installed by using inversion or pulled in place technique at the construction site and the thermosetting resin is cured in place to bond the liner tightly to the existing pipe[1]. Thus, the CIPP liner can be installed remotely inside existing underground cast-iron pipelines with minimum outside disturbance through trenchless construction procedures[7, 8]. The most commonly used Starline HPL-G liner can rehabilitate a high-pressure pipeline with a diameter up to 24 inches with existing and future pitting corrosion of up to 2 inches or cracks up to 1 inch under an operating pressure up to 250 psig[9]. The Starline HPL-G liners have shown efficiencies in removing those pipeline defects fast, while accommodating bends and changes at the pipe cross-section of the pipe. Previous studies focused on developing advanced equipment and installation techniques, establishing limit state design approaches for the linings[10, 11], and quantifying the effects of imperfections that may result from the installation process.

2.2.2 Recent Development of Vitrimers and Their Application as Self-Healing Polymer

For the thermosetting resins used for the CIPP liners, there are three common types including epoxy resin, unsaturated polyester, and vinyl ester resin as the chemical resistance liner for the highly corrosive condition in need of chemical resistance liner. The epoxy resin is widely applied due to its unique properties such as low shrinkage, low viscosity, long pot life, satisfactory wetting, excellent adhesion to various substrates (metal, concrete, and plastic), and desired thermal and mechanical properties. However, the curing for the conventional anhydride cured epoxy resin is slow, incomplete, and complicated in the absence of catalysts (for example, zinc salts). In addition, it is a formidable challenge to heal/repair the microcracks after the linings are in place since thermoset materials become infusible and insoluble once they are cured and cross-linked, which makes them difficult to weld and repair. Therefore, if the CIPP liner is damaged and fails to further protect the pipe from leakage, the old liner needs to be removed and replaced with a new liner, which is often very difficult because of the strong adhesion at the interface. After the removal, the irreversible covalent networks of the conventional epoxy resins in the old liner prevent the old thermoset resins from being reprocessed, recycled, reshaped, remolded and reconfigured. Most of the discarded thermoset epoxies and polyurethanes are disposed of by incineration or landfill, which in return has brought forth severe environmental pollutions and wasting of resources[12]. Thus, the needs to develop more environmentally friendly or reusable epoxy have attracted significant attentions in investigating vitrimer polymers.

Vitrimers are crosslinked polymers in which the crosslinks are made of dynamic covalent bonds (rather than permanent covalent bonds found in traditional thermoset polymers). These bonds allow the formation of covalent adaptable networks (CANs) inside vitrimers and impart the material self-healing, recyclable, malleable, and reprocessable capabilities when stimulated (by heat, for instance). Above the vitrimer temperature Tv (or topology freezing temperature), the dynamic bonds in vitrimers can exchange (the initial bond is broken upon the formation of a new covalent bond at a different site), which leads to a significant decrease in material viscosity while still being able to retain network integrity and mechanical stability of the material (Figure 1, Ref.[13]). This behavior is in sharp contrast to the traditional thermoset polymers, in which the crosslinks are permanent and therefore do not allow softening of the materials.

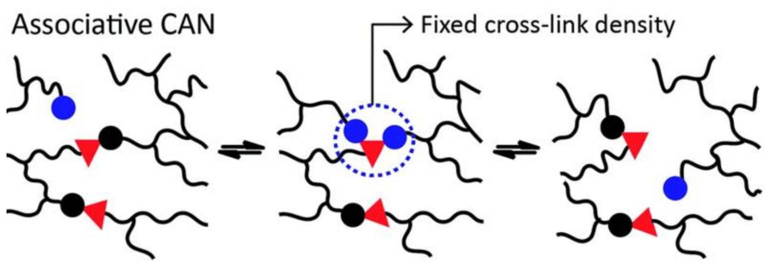

Figure 1. Illustration of the modification of network topology in vitrimers when the temperature is above the vitrimer temperature Tv[13]

In the last ten years, quite a few chemistries have been developed to produce dynamic covalent bonds and enable the bond exchange processes, including transesterification[14, 15], transamination of vinylogous urethanes[16, 17], transalkylation[18, 19], disulfide exchange[20, 21], and imine exchange[22, 23]. Figure 2 shows several commonly used reactions in the bond exchange processes[24].

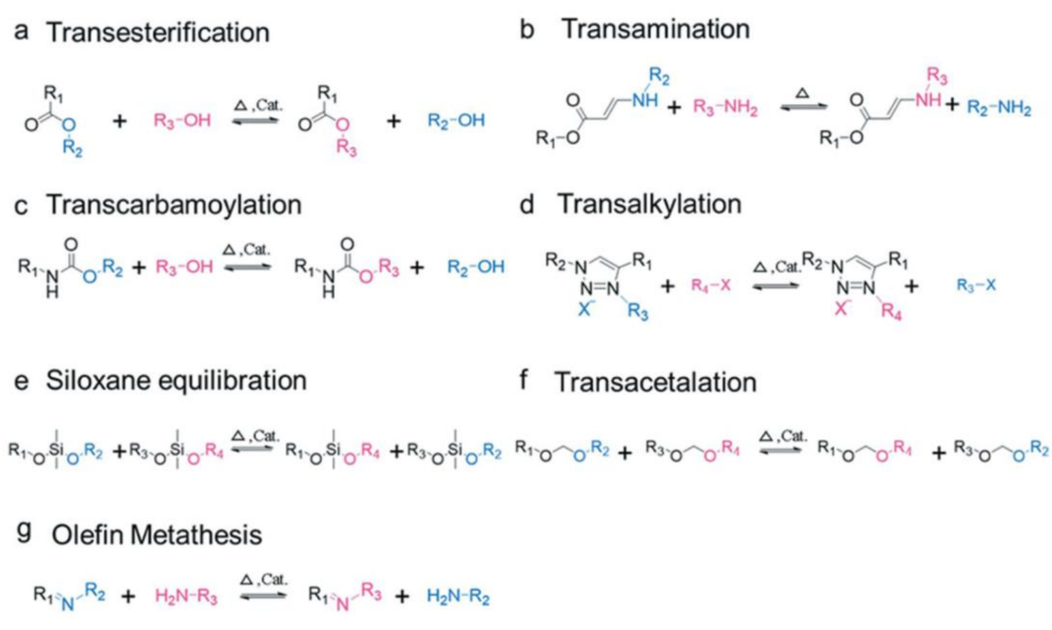

Figure 2. Several common covalent exchange processes[24].

Transesterification-based vitrimers undergo bond exchange processes through dehydration condensation and hydrolysis of the carboxyl and hydroxyl groups as shown in Figure 2a. The rate of transesterification is almost zero at room temperature, and this network exhibits characteristics resembling those of conventional chemically crosslinked networks, such as strong mechanical stability without creep. The quick transesterification reaction, however, allows such vitrimers to relax after heating by rearranging the network structure[25]. The transamination-based vitrimers (Figure 2b) carry out the Michael addition-based exchange of urethane and ammonia at a high temperature. Catalysts are not necessary for the reaction process. However, it is important to consider the amine's network stability since amine oxidative degradation reduces the material's durability[13]. The vitrimers based on transcarbamoylation (Figure 2c) achieve exchange by a carbamate reaction, but the reaction is sluggish and has undesirable side effects. A typical transalkylation-based vitrimer (Figure 2d) is created by polymerizing an alkylating reagent with a bifunctional group and an azide-alkyne monomer in addition. However, transfer agents are difficult to industrialize due to their low scalability, high cost, and high toxicity of azide and alkylating agents[19, 25]. The silanol groups or silanols are added to or removed from siloxane molecules to create the siloxane equilibration-based vitrimers (Figure 2e), but adverse reactions including hydrolysis degradation, heat cyclization, and depolymerization might damage the topological network structure. The combination of acetals with alcohols results in the transacetalation based vitrimers (Figure 2f). The imine-amine reversible exchange and imine reversible exchange are used to construct the olefin metathesis-based vitrimers (Figure 2g), however, the polyimine network is susceptible to water, limiting the uses of this kind of material. It should be emphasized that additional dissociative dynamic covalent links, such as disulfide bonds (S-S) and diselenide bonds (Se-Se), have also been used in the synthesis of DCBs in addition to the associative dynamic covalent bonds for vitrimers that were addressed above. The exchange mechanism entails the insertion or removal of replacement by free thiols through a conjugate exchange process[26]. Due to their shared chemistry and chalcogen group membership in the periodic table, diselenide, and disulfide bonds have a comparable exchange mechanism.

Self-healing coating: A self-repairing material should ideally be able to sustain an endless number of healing cycles without losing characteristics or consistency. The introduction of CANs paved the way for intrinsically healable and adaptable materials that frequently require only a little amount of external intervention via temperature or light[27]. Recently, Ma et al.[28] developed an ultra-thin self-healing vitrimer coating for durable hydrophobicity. The vitrimer was synthesized using poly(dimethyl siloxane) diol and boric acid and the self-healing was attributed to the associative B-O bond exchanges. The coating exhibited long-term hydrophobicity and optical transparency after scratching, cutting, and indenting. The polydimethylsiloxane vitrimer thin film could be deposited on a variety of substrates via scalable dip-coating.

Recyclability of vitrimers: Vitrimer products are ground into a fine powder and hot pressed back into new products. In this process, high pressures are necessary to fuse the particles together because increased contact at high temperatures results in more effective bond exchanges[29]. Ruiz de Luzuriaga et al.[30] created a fiber-reinforced polymer composite using DGEBA and an aromatic disulfide hardener (FRPC). They found that the powder derived from the control (DGEBA and aromatic diamine) could not be recycled to fresh specimens for tensile testing (under the conditions of 200 °C, 100 bar, and 5 min). On the contrary, utilizing an aromatic diamine with reversible disulfide bonds allowed for a self-repairing treatment, and the samples recovered their original mechanical characteristics completely. Delahaye et al.[31] investigated the recycling of catalyst-free polyester vitrimers. Specimens were ground into particles with sizes of around 1 mm, and the resultant particles were hot-pressed at 150°C for 60 minutes to produce translucent specimens for retesting. This recycling process was repeated three times, and each time the recycled samples showed tensile properties similar to the original material. In 2021, Feng & Li[32] published a covalent adaptive network (i.e. polyethylene CAN) based on hydroxy phosphate, which demonstrated high strength, recyclability, shape memory, and fire resistance capabilities. A large amount of hydrogen bonding in PE-CAN increased its toughness (5.44 MJ/m3) at ambient temperature. The quick exchange reaction between the phosphate ester and the neighboring hydroxyl group at roughly 100°C results in nearly 100% recycling efficiency of the material.

Biobased vitrimer: The number of papers on biobased vitrimers has dramatically increased during the past five years because the combination of vitrimers and biobased polymers enables the design of high-performance and sustainable materials. The world's most significant renewable source of aromatic polymers is lignin, which can be found in high concentrations in wood (up to 30%wt), as well as in the stems of annual plants, herbs, and nut shells. Lignin also exhibits great functionality because of its abundant aliphatic and aromatic hydroxyl (OH) groups. A few attempts have been made to create lignin-based vitrimers in recent years. In two separate experiments, Kraft lignin (KL) was utilized to crosslink diepoxy monomers with polycarboxylic acids, resulting in the production of transesterification vitrimers with a zinc catalyst. KL naturally has a small number of carboxylic acid (COOH) groupings. Two different methods were used to raise the COOH content of KL (Figure 3, Ref.[33]).

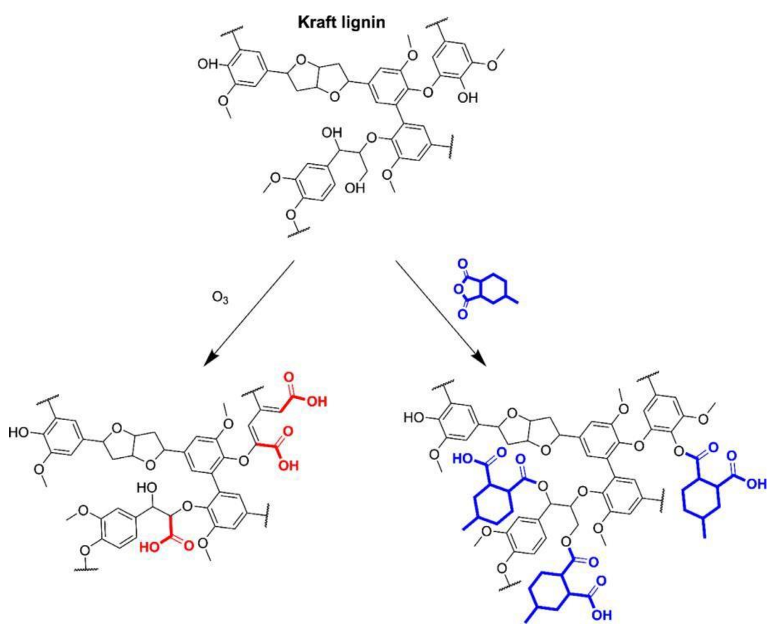

Figure 3. Chemical modifications of Kraft lignin to introduce COOH groups[33].

By using ozonation to modify KL, Zhang et al.[34] created COOH groups by the opening of phenolic rings and the oxidation of aliphatic OH groups. The lignin depolymerization that is known to happen with prolonged ozone treatments appears to be avoided by using very modest settings[33]. Another significant source of aromaticity is furans, and many building blocks can be made from biobased materials. Recently, 2,5-furandicarboxaldehyde (FDC) has been used to create aromatic polyimine (PI) vitrimers that are completely biobased. The vitrimers are derived from carbohydrates and fatty acid-based amines, making them highly desirable for the creation of sustainable biobased goods. The created material demonstrated excellent stability at 120 °C, a Tg of -10 °C, quick stress relaxation, and good viscoelastic characteristics. They may be completely depolymerized for the recovery of the building block in butylamine owing to the transimination process. The materials also demonstrated good reprocessability as they underwent three recycling cycles and still maintain good mechanical properties[35].

UV- cured Vitrimer: UV curing or combined UV & thermal curing has become increasingly popular due to its low cost, simple operation, and efficiency. Feng & Li[36] developed a UV-curable phosphate diester-based acrylate cross-linker without the need for a catalyst. The phosphate diesters act as reversible covalent bonds, hydrogen bonding ligands, and flame-resistant structures, whilst the acrylate groups act as UV-curable units and co-reactants in transesterification. Due to the plentiful hydrogen bonding between P-OH and C=O structures, an intrinsically flame-retardant and mechanically robust dynamic network was created after the simple UV curing. This phosphate diester-based mixed transesterification idea may also be applied to other thermally cured polymer systems.

Fei et al.[32] used glycidyl methacrylate and dimer acid from vegetable oils to create bio-based UV-curable dimethacrylate molecules. The characteristics of the cross-linked polymer can be tailored by varying the chain segment length and pliability between the two methacrylate groups. The material showed a tensile strength of up to 9.2 MPa and an elongation at break up to 66.4%. The material was repairable at high temperatures (>160 °C) due to the thermally induced dynamic transesterification reaction (DTER) between hydroxyl groups and ester bonds in the network structure. The material can be used as a 3D printing resin and due to its vitrimer behavior, the printed objects exhibited welding and shape-changing abilities.

Role of fillers in vitrimer applicability: Hubbard et al.[37] studied the effects of fillers on the performance of vitrimers, including their thermomechanical characteristics, self-healing, and shape-processing capabilities. They showed that, regardless of filler type, filler concentration and dispersion played important roles in reducing material creep and increasing Tv and mechanical characteristics (e.g., modulus and strength). They also found that the inclusion of filler had no discernible effect on composite shape memory or shape reconfigurability, but it did facilitate self-healing. Vitrimer composites enable a level of tunability previously unattainable through chemical changes alone. Composite design with tailorable Tv, strength, and processability is attainable by altering filler type, concentration, and dispersion quality, making it ideal for a wide range of applications.

The potential to prolong the service of thermosetting polymers by self-healing and recycling is unquestionably exciting, especially in light of the growing concern for environmental concerns and dangerous chemical waste. Vitrimers are a novel class of thermosets having the capacity to flow above a specific characteristic temperature given by the chemistry involved. They were just recently presented to the scientific world, less than twelve years ago. Covalent bond exchange, such as transesterification, transamination, or disulfide metathesis, is used to produce this feature. The basic idea behind vitrimers is a network that may self-arrange in response to stimulation, preferably without losing its integrity or experiencing any undesirable side effects. Additionally, the use of bio-based monomers for the creation of vitrimers has drawn attention as a potential solution to the issue of the depletion of petroleum resources. The molecular-level control of the fundamental physics and flow characteristics of vitrimers, such as stress-relaxation and linear viscoelasticity, have also been researched for the practical application of the vitrimer idea since these qualities are strongly connected to material processing. Since vitrimers are still a relatively new technology, further development of vitrimers, including design, modification of properties, functionalization, and discovery of new application domains (such as for shape memory polymers and 3D printer resin), is highly advantageous and can unquestionably result in the realization of a sustainable society.

2.2.2 High-performance Modified Epoxy

Pipeline linings used for the rehabilitation of cast-iron natural gas pipeline are required to operate under high internal pressures up to 350 psig. CIPP Liners with smaller amounts of resin and a smaller thickness reduce on-site work hours as the curing speed is faster and is economical due to the low cost of maintaining the heat required for curing decreases. The thickness of the CIPP liner depends on multiple factors including long-term and short-term tensile strength, flexural strength, and flexural modulus. Among them, the flexural structural property and Creep Retention Factor (CRF) of the liner are of great importance as a higher strength of the CIPP liner requires a thinner liner[38], which varies significantly by resin types and manufacturers. Figure 4 shows the required CRF for liners reported in various different stndards[38]. The ASTM F1216[39] adopts a long-term flexural modulus for calculation of CIPP liner thickness design by using CRF value for the CIPP liner design. A CRF of 0.5 (50% retention of short-term flexural modulus) is typically adopted as an industry standard practice for water pipelines. CRF 0.5 is still used for non-reinforced CIPP using standard polyester resin system. Such traditional non-reinforced CIPP liners usually have a large thickness because the minimum requirement for the flexural property is relatively low and a relatively low CRF.

Various resins have been developed and used for CIPP liners, including polyester resin, vinyl ester resin, and epoxy pipelines[38]. The polyester resin is the most common resin for rehabilitation of municipal sewage pipelines, which contains Styrene to help the polymerization process when heated. The vinyl ester resins have higher corrosion and chemical resistance than polyester resin[38], which are most commonly applied for rehabilitation of industrial pipelines with higher temperature range, ductility, and good curing characteristics in presence of water. However, it is more expensive than the polyester resins. The epoxy resin with high chemical resistance as well is commonly used for rehabilitation of pressure pipelines and suitable for potable water application. In addition, some other resins such as no styrene-based resin and silicate resin without styrene odor[40] have also been investigated for some applications of CIPP liners.

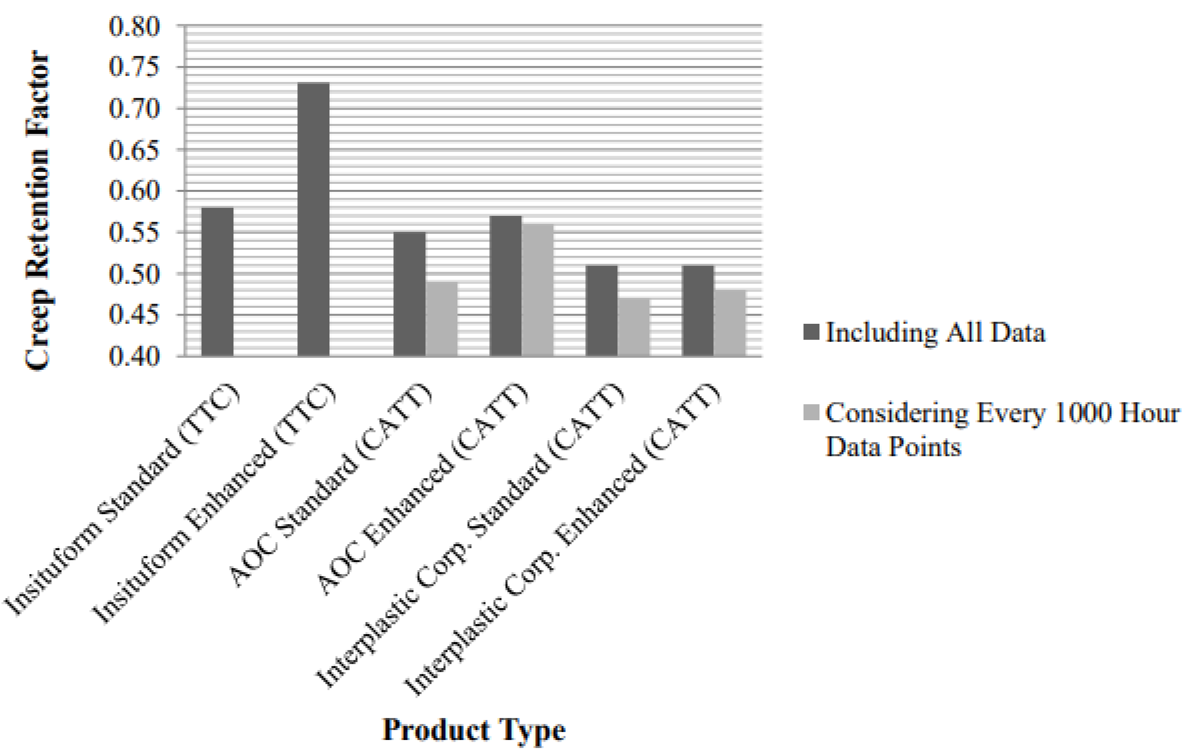

Figure 4 Comparison of creep factors reported in various standards

Fiber Reinforced CIPP: Since a reinforced CIPP structure retains higher CRF values, they have been investigated for high strength CIPP liners that has a thinner thickness and is more cost-effective. North American Society for Trenchless Technology (NASTT)[40] present typical CIPP mechanical property values for gravity pipelines in good practice guidelines. They suggest CRF up to 80 percent (CRF 0.8) for highly reinforced CIPP. Glass fiber has been used as a lightweight reinforcement material for the CIPP liner[40, 41]. The glass fiber reinforced polymer (GRP) was used instead of needle felt layer and was found to increase the flexural strength and modulus. The CIPP liner samples in these studies were fabricated by combining the liner materials as presented in Table 1[42]. Based on Table 1, it can be seen that most of the fiber reinforced CIPP investigated previously focused on the polyester resins for water or sewage pipes. Short- and long-term tests performed on the samples following ASTM D790 showed that the flexural strength and flexural modulus of the glass fiber reinforced CIPP increased significantly than the American Society for Testing Materials minimum criteria for CIPP short-term properties. The maximum CRF was higher than 0.64, which can reduce the design thickness of the CIPP by up to 54%. The structural characteristics also improved when glass fibers were mixed with traditional CIPP liner, making it possible to reduce the thickness by 30%[41]. However, a long-term creep test only confirms CRF. Nassar and Yousef [43] experimented and analyzed a long-term buckling behavior of a pipe under external hydrostatic pressure for at least 50 years. Their work showed that the current regression-based prediction for the long-term failure analysis is conservative and actual CIPP behavior is less likely failed with over 80 percent survival probability.

Table 1 Summary of materials and its characteristics for CIPP liner used [42]

Group Number	Composition Criteria	Materials	Thickness	Unit Weight
1	Polyester Resin	Unsaturated Polyester with styrene monomer for CIPP (UP)	N/A	1.13 g/cm^3
2	Glass Fiber and Polyester Resin	Thin Roving Cross Glass Fiber Mat (TG)	0.5 mm	0.9 g/cm^3
		Roving Cross Glass Fiber and Chopped Strand Mat (G)	1.0 mm	0.96 g/cm^3
		Unsaturated Polyester with styrene monomer for CIPP (UP)	N/A	1.13 g/cm^3
3	Carbon Fiber, Glass Fiber, and polyester resin	Roving Cross Glass Fiber and Chopped Strand Mat (G)	1.0 mm	0.96 g/cm^3
		Unidirectional Carbon Strands Mat (C)	<0.5 mm	1.81 g/cm^3
		Unsaturated Polyester with styrene monomer for CIPP (UP)	N/A	1.13 g/cm^3
4	Glass fiber, Polyester Felt, and Polyester Resin	Roving Cross Glass Fiber and Chopped Strand Mat (G)	1.0 mm	0.96 g/cm^3
		Polyester Needle felt (F)	2.0 mm	0.3055 g/cm^3
		Unsaturated Polyester with styrene monomer for CIPP (UP)	N/A	1.13 g/cm^3
5	Glass fiber, Thin polyester Fabric, and polyester resin	Roving Cross Glass Fiber and Chopped Strand Mat (G)	1.0 mm	0.96 g/cm^3
		Thin Polyester Woven Fabric (TF)	<0.5 mm	0.637 g/cm^3
		Unsaturated Polyester with styrene monomer for CIPP (UP)	N/A	1.13 g/cm^3

In addition to glass fiber reinforcement, carbon fibers in epoxy[44,] can also improve the flexural properties at a relatively higher cost. Carbon fiber fabrics and materials are already used extensively in the aerospace and defense industries, as there can be some major benefits to using carbon fiber systems due to their superior physical properties[45]. In recent decade, the use of carbon fiber has begun to be used more extensively in small-diameter lining systems using CIPP[44]. In addition, the carbon fiber reinforcement has also been investigated to be added to the traditional glass fiber reinforced epoxy CIPP for fire suppression lines that needs to have a minimum safety factor of 4 with burst pressure higher than 600 psi and temperatures as high as 150°F[46]. The glass fiber or carbon fiber reinforced liners are mainly installed by the pull-in installation method, and this application requires a calibration tube for the curing purpose. The glass reinforced CIPP liner has considerably high strength than the conventional felt based CIPP liner. However, the use of a calibration tube makes it challenging to improve construction productivity and cost competitiveness[40, 41].

Carbon Nanotube Reinforced Epoxy: Compared to polyester resins, epoxy resins with high strength-to-weight ratio, good environmental stability, and ease of application have been popularly applied in CIPP liners for high pressure application such as oil and natural gas pipelines. Although no applications of incorporating nanofillers in epoxy has been investigated in CIPP linear, the addition of a small proportion of nanofillers such as carbon nanotubes (CNTs), graphene nanoplatelets (GNP), and single-walled carbon nanohorns (CNH) [47] inside epoxy resins for other applications have been investigated. Among various nanofillers, carbon nanotubes (CNTs) with extraordinarily high tensile strength and young's modulus, are expected to be promising additives for polymer reinforcement [48-50], which could considerably improve mechanical and adhesion properties of CNTs reinforced epoxy resin, with respect to strength, toughness, and bonding.

However, as a nanofiller, CNTs are difficult to be uniformly and evenly dispersed in the epoxy matrix. It is not only because of the relatively high viscosity of the epoxy resin, but also owing to the extremely high aspect ratios and extremely large surface areas of CNTs, which, in return, result in strong Van der Waals forces on the surface[51]. Without any external stimulus to break the intermodular interactions, CNTs are more likely to agglomerate and entangle into CNT clusters which normally weaken the strength, cause stress concentration and other detrimental effects as defects or imperfections[51, 52]. Thus, the reinforcing efficiency of CNTs reinforced epoxy composites are highly restricted by the agglomeration and entanglement of CNTs, and a uniform dispersion has become a critical issue and a prerequisite to optimizing the desired performances of CNTs reinforced epoxy composites[53, 54]. In addition, the nonuniformity and potential inconsistency of the resulted epoxy resins have limited the application of CNT reinforced epoxy resin as adhesive for CIPP structural lining materials. Recently, a new surface treatment method using carboxymethyl cellulose (CMC) to treat the CNTs which has been approved for a better dispersion in polymer and cementitious materials[55, 56]. CMC is a water dispersible cellulose derivative, and its sodium salt has been exclusively used in food, cosmetic and pharmaceutical industries as a thicker stabilizer or binder[55]. Moreover, CMC is an environmental-friendly, biocompatible, and disposable material without any harsh chemicals, which makes it even more favorable than some other solvents. The CMC surface treatment may bring a potential for improving the uniformity of the CNT reinforced epoxy composites for application in CIPP liners. The combination of glass or carbon fiber reinforcement with CNT reinforcement in epoxy resins for CIPP liners may be potentially a solution for high strength CIPP liners, however, not yet investigated, and requires further studies.

2.2.3 Chemical Analysis of Surface Bonding and Permeability

To analyze the surface bonding of the CNT-modified healable epoxy resin, it is needed to analyze the chemistry at the CNT-modified healable epoxy resin/cast-iron interface and to evaluate the permeability of methane, carbon dioxide and their mixtures over a range of temperatures and pressures which are of interest to field applications.

Cast-Iron Facets. The body-centered cubic (BCC) crystal structure of pure Fe will be utilized to construct the cast-iron facets. El-Lateef and co-authors studied the poly-(hydrazinylazo) thiazoles as potent corrosion inhibitors for cast iron-carbon alloy. In their density functional theory (DFT) and Monte Carlo (MC) calculations, the Fe(110) facet was adopted[57]. It is worth pointing out that for cubic materials, the most prevalent cleavage planes are the (100) planes. For the investigation of cleavage and inherent plasticity, the deformation such as crack usually lies parallel to high-symmetric lattice directions. For cast iron, planes of (100), (110), (101) and (111) have been studied for the crack cleavage and fracture development[58-60]. The order of surface energy of iron surfaces is Fe(110) < Fe(100) < Fe(111), making Fe(110) to be the most stable, followed by Fe(100) and Fe(111) facets[61]. Top views of most densely packed surfaces of bcc structure are shown in Figure 5. In a recent review by Haris and co-authors[62], the lowest energy configuration of Fe(110) surface has been widely adopted for computational studies. In this study, we will also use BCC Fe(110) for the model development.

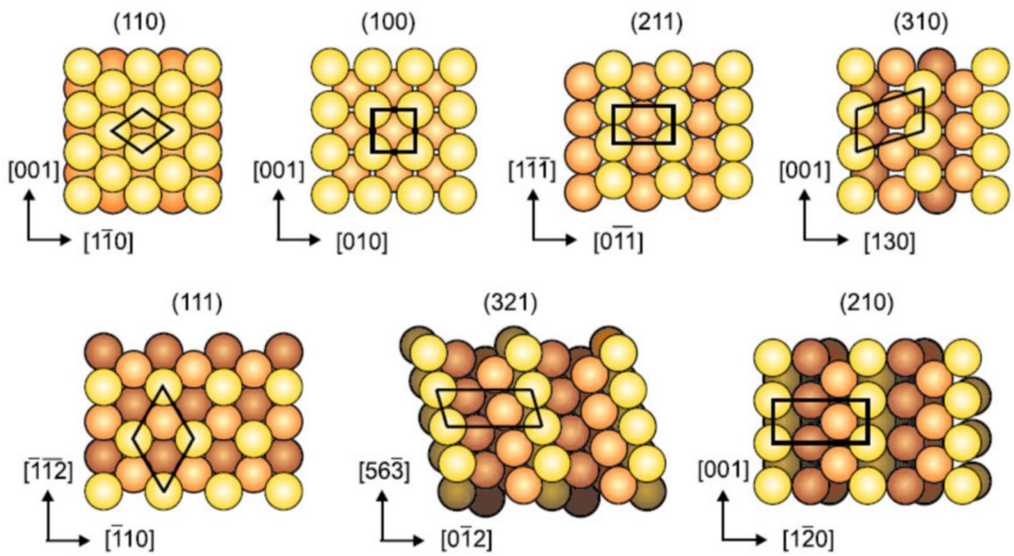

Figure 5. Top view of most densely packed surfaces of bcc structure. The surface unit cells applied in the calculations are shown. The shading of layers is increasing with layer depth. [61]

Carbon Nanotube. Carbon nanotubes (CNTs) represent a material that has been extensively studied in both theory and experimental practice ever since their discovery in 1991. The extraordinary mechanical properties and fiber like structure of CNTs have made them a promising reinforcing component for nanostructures and nanomaterials. CNTs have Young's modulus in the range of 1-6 TPa, tensile strength in the range of 20-60 GPa and strain carrying capacity of 12%. Compared with steel, the commonly produced multi-walled carbon nanotubes (MWCNTs) has modulus of elasticity approximately 5 times higher, tensile strength 100 times larger, can reach elastic strain capacities 60 times greater, and yet has a specific gravity only one sixth that of steel[63]. In this study, we will firstly evaluate single-walled carbon nanotubes (SWCNTs). As shown in Figure 6, armchair and zigzag types of SWCNTs will be constructed, with diameters ranging from 8.1 Å to 13.5 Å. Investigations on other geometric arrangements, such as chirality multi-walled, and functionalized CNTs will be planned as well.

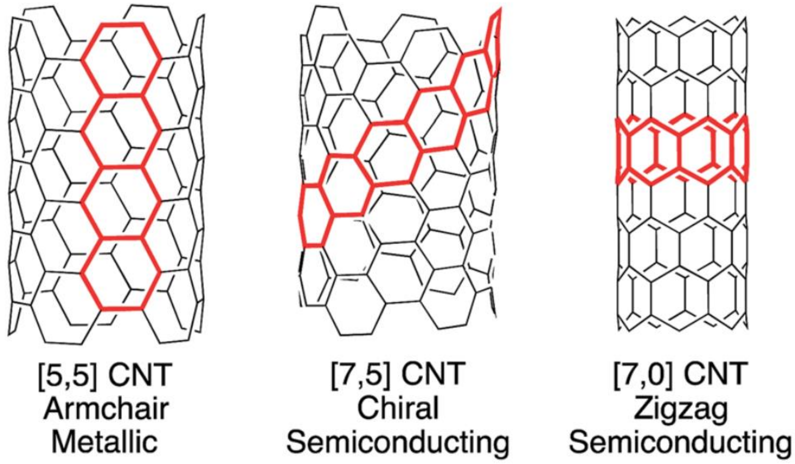

Figure 6. Carbon nanotubes are classified as armchair, chiral, or zigzag based upon their structure[63].

CNT-Reinforced Self-healable Epoxy Resin. Self-healable polymers promise reduction in the maintenance cost and therefore enables a prolonged lifetime with a better function of reshaping and recyclability. Designing materials capable of self-healing needs to overcome two general challenges. The first challenge comes from sorption of molecules into polymer structures, which changes polymer structures, thus promoting polymer plasticization. This process is typically associated with a decrease in the glass transition temperature (T_g) of the polymer. The second challenge is the high relative permittivity of environmental water, which weakens the mechanical properties of the polymers. The self-healing property can be manipulated by incorporating materials such as CNTs into the matrix of the self-healing polymer. In 2011, Montarnal and co-authors[64] designed epoxy designed epoxy networks with reversible covalent bonds and named them "vitrimers", see Figure 7. Epoxy vitrimers can maintain a constant polymer cross-link density while exhibiting flow properties similar to those of silica when heated during material processing. This new epoxy network can be readily scaled up for applications and generalized to other chemistries. Besides the vitrimer polymers based on β-hydroxy esters, a series of other self-healable polymers have been developed in recent years through various exchangeable chemical reactions, for example, disulfide exchange[65], imine exchange[66], siloxane silanol exchange[67], olefin translocation[68], etc. More detailed discussions are available in recent reviews[69-72].

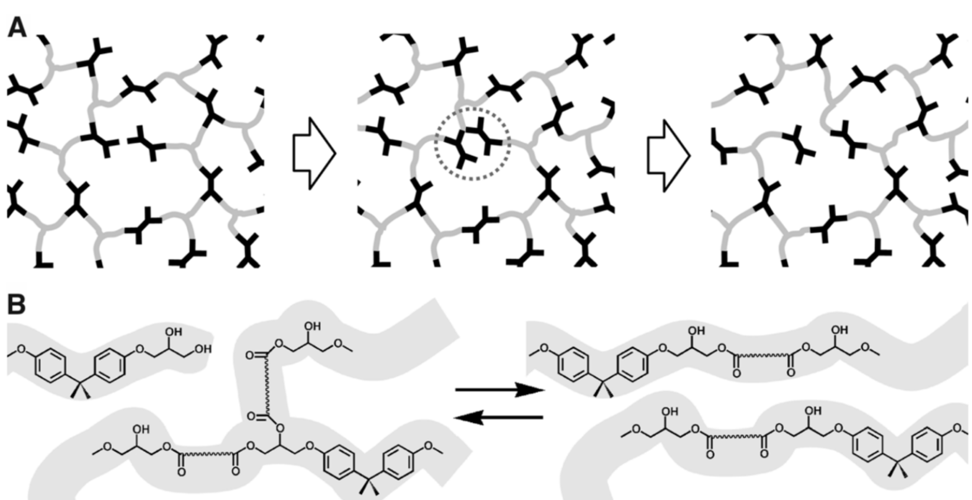

Figure 7. Topological rearrangements via exchange reactions preserving the network integrity. (A) Schematic view of a network with exchange processes that preserve the total number of links and average

functionality of cross-links. The middle image illustrates that the exchange does not require depolymerization in the intermediate step. (B) Exchange process via transesterification in hydroxy-ester networks.[64]

As for the computational studies, Zhao and co-workers performed molecular dynamics (MD) simulation of a model vitrimer system[73]. They constructed the dynamic covalent network by linear polymer chains, and investigated the structural, mechanical, and reprocessing properties of the model vitrimers. Yang et al. performed MD simulations to understand the surface welding and shape memory behaviors of the covalent adaptable network polymers[74]. They reported that the welded networks can fully recover the mechanical properties of the fresh network, and that the glass transition temperature of welded network varies with the weight fractions of epoxy monomers. A similar MD simulation study of the self-healing behavior of disulfide bond exchange reactions was reported by Zheng and co-workers[75]. It is popular to set up the model system, as shown in Figure 8, for the study of thermally reversible linkages in crosslinked polymer networks[76].

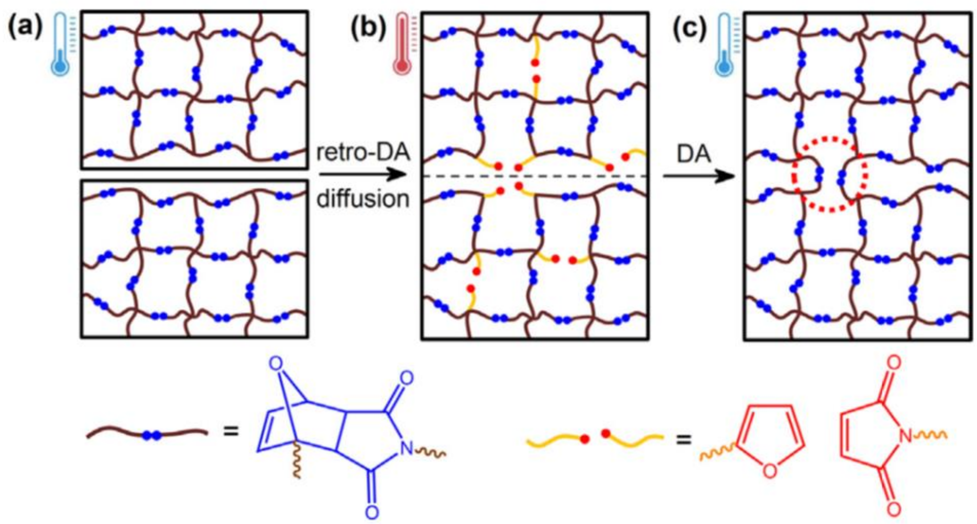

Figure 8. Schematic illustrations of the processes involved in surface welding of the Diels-Alder (DA) networks. (a) Two separate DA networks brought in contact; (b) de-polymerization due to the retro-DA reaction at elevated temperatures; (c) re-polymerization and formation of interfacial linkages (as highlighted by dash line circle) due to the DA reaction at relative low temperatures. The blue and red dots represent DA adducts and pendent furan/maleimide groups, respectively. The orange lines represent dangling chains.[76]

Methods and Computational Details: (a) Force Field. The COMPASS (Condensed-Phase Optimized Molecular Potentials for Atomistic Simulation Studies) force field, which is based on the Polymer Consistent Force Field (PCFF)[77, 78] , will be applied to describe all studied polymer segments and their interactions in the MD simulations. This force field is parameterized and validated using condensed-phase properties and various *ab initio* and empirical data of various molecules. It can predict various properties for a wide range of polymer molecules. The free volume will be evaluated by the technique of Voronoi tessellation of space[79] and by enumeration of the cavities[80] formed with hard sphere probes. The expected outcome would be two-fold: atomistic composite model and its structural dependence on temperature.

(b) Binding at the Interface. In this project, we seek to understand the formation mechanism and the interface chemistry of the CNT-modified healable epoxy resin/cast-iron model. The nature of the interface and the bonding between segments of epoxy resin and the cast-iron, the Fe(110) facet, will be also explored via *ab initio* density functional theory (DFT) calculations. Due to the computational expense of DFT calculations, we will limit our calculations to only the atoms at the interface. This is a suitable approximation since strong bonding is typically determined by forces that are very short-range in nature. We expect to identify minimum energy structures of the models and their structural dependence on temperature. It is worth noting that the free volume and its change as a function of temperature could be characterized by experiments, such as positron annihilation lifetime measurement. Those experimental results can be used as reference to modify the simulation protocol and the model setup, such as the mass ratio of CNT/epoxy resin/cast-iron and the initial configuration of epoxy resin with respect to cast iron. The VASP software, with the van der Waals interaction correction, will be applied for those DFT calculations[81, 82].

(c) Structural and Mechanical Properties of the Interface Model. In this work, we plan to calculate the stress-strain properties of the interface model. The Young's modulus defines the relationship between stress (force per unit area) and strain (proportional deformation) in the linear elasticity regime of a uniaxial deformation. A larger Young's modulus suggests a better stiffness of a material. Young's modulus could be experimentally determined via X-ray diffraction or Raman spectroscopy. Computationally, several methods have been proposed to calculate this elastic modulus, as discussed in our previous publications[64, 65]. One method is to enlarge the simulation box length repeatedly by a small amount, along the axis where the stress is applied. The simulation system is then reoptimized at each new fixed cell unit. Another method is to allow the simulation box to elongate continuously at a defined strain rate for a uniaxial tensile deformation. We also utilized the second method to monitor the uniaxial tensile deformation of cellulous network at three different strain rates[83], see Figure 9. In those simulations, the tensile stress is the negative value of pressure along the corresponding direction. The strain is then calculated by the amount of the length change for that direction. Young's modulus (E) is the ratio of tensile stress ($\sigma(\varepsilon)$) and strain ε, $E = \sigma(\varepsilon)/\varepsilon$. From the stress−strain diagram, the point of yielding is estimated by the offset yield method, also known as 0.2% offset yield strength. While the yield strength could be obtained by drawing through the point of the horizontal axis of $\varepsilon = 0.2\%$, a line parallel to the initial straight-line portion in the stress−strain diagram.

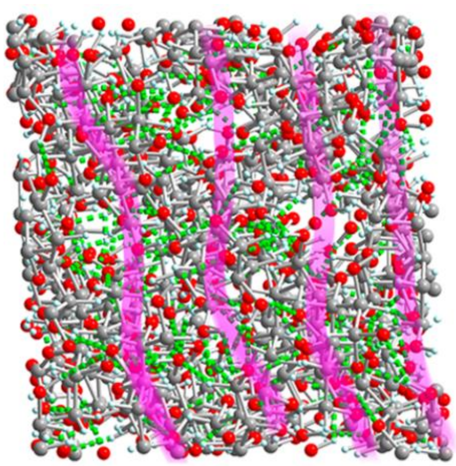

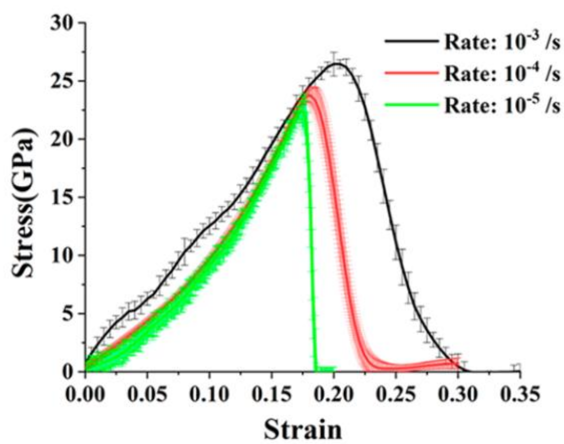

Figure 9. (Left) Schematic illustrations of cellulose network uniaxial tensile deformation; (Right) The stress−strain diagram of cellulose at 300 K and different strain rates.[83]

(d) Permeability Calculations. As discussed in the recent review[84], the evaluation of permeability of polymer networks can be achieved by conventional MD simulations. The permeabilities can be evaluated directly by Fick's First Law, transition rates, and a global Bayesian analysis of the inhomogeneous solubility-diffusion model. In this project, we will employ MD simulations to study simultaneous adsorption, diffusion and separation of CH_4, CO_2 and their mixtures in the constructured composite models. Those calculation results will be supplied to and be iterated with both experimental results, material design and process optimization. It should be noted that, unless necessary and evidenced by experimental results, we'll adopt rigid composite models in the permeability studies. The reaction or the structural collapse of the composite will be neglected. CH_4 will be described by the simplest Lennard-Jones representation according to the OPLS parametrization once used by Grade et al.[85] CO_2 will be described by the EPM2 model[86]. Properties, such as self-diffusion coefficient, molecular orientation and density profile, the atomic mean-square fluctuation amplitudes, permeability and selectivity will be calculated and compared with experiments whenever possible. Such fundamental understanding of the dynamics process will also provide insight on how the interaction, permeability, and selectivity change as a function of time, temperature and pressure. For dynamic properties, it is necessary that the simulations have adequately sampled the configuration space and have collected sufficient dynamic trajectories. Both CPU and GPU versions of LAMMPS[87, 88] will be tested and applied for those MD calculations.

2.2.4 Assessment and Monitoring of CIPP Liners

Once the CIPP lining has been fully installed, the rehabilitated pipelines need to be certified or evaluated. There are various technologies can be used to evaluate, assess, and certify the CIPP liners. This section reviews the current state-of-practice for the liner inspection and monitoring.

Visual Inspection: Typically, the rehabilitated pipeline sections were evaluated using only visual inspection following ASTM F1743 or closed-circuit television (CCTV, Figure 10a[89]) cameras before and immediately following the lining of a pipe to ensure the quality of the CIPP lined pipes meets the standard for large and small projects [90]. Compared with a visual inspection, the CCTV inspection uses recorded videos or images (Figure 10b[90]) to find defects in CIPP liner, which has a relatively low cost and is familiar to agencies or operators. It can also uncover other operating problems such as blockages and provide broad coverage of relined sections within an agency, leading to statistically meaningful results. However, CCTV also has its disadvantages. For example, it can only identify deteriorations or defects that are easily identified visually, and it is not possible to evaluate intermediate stages of deteriorations or liner distortions.

Figure 10. (a) Example CCTV[89] and (b) image of defects recorded by CCTV for pipeline liners[90]

FELL Inspection: Recognizing the growing use of CIPP liners and the inability of CCTV inspection to accurately or consistently certify trenchless rehabilitation as defect-free, Electro Scan Inc. developed the focused electrode leak location (FELL) inspection and low voltage conductivity (LVC) as shown in Figure 11 to test, certify, and accept CIPP lining projects in 2012[90, 91]. Previous practice has verified that the FELL technology can consistently find defects missed by the CCTV inspection, such as wrinkles, accelerant burns, bad resin, weak liner, overcooked liner, defective epoxy, bad connections, annular space, infiltration spotting, sag in liner, open joint, blistering, etc.[90] However, similar to the CCTV, the FELL is also an inline technology that will be applied upon request and not an online technology for continuous condition assessments.

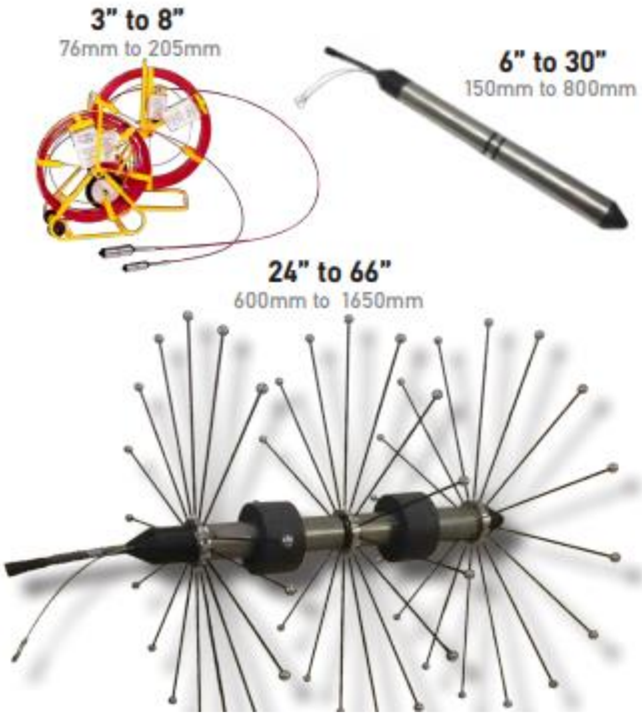

Figure 11. Example FELL (Electro Scan Inc.) [90]

It is known that during cure, the exothermic reaction of the resin in the liner can occur on a small scale, and non-uniformly with respect to time and distance. Thus, it is of great importance to monitor the temperature along the CIPP liner during curing process, instead of measuring the temperature only at the end point. To monitor the temperature changes of the CIPP curing process, recently, a new technology has been developed to monitor temperature readings along a full segment of pipe during the curing of the CIPP (cured-in-place-pipe) lining process[92]. The procedure uses sensors strung by cable inside the pipe to be relined before the liner is inserted into the pipe. After the liner is in place and the curing process initiated by steam, water or ultra-violate light, the sensors read and transmit exothermic conditions to an on-site computer, smart phones can also be used. To ensure proper and complete curing, it is best to know the temperature between the liner and host pipe for the complete length of the pipe. Sensors are installed every 10 to 20 feet along the host pipe as the resin-based liner is cured. The distance between sensors varies with diameters of host pipes. Knowing the temperature every 20 feet or less will help reduce the risk of curing failure. Software also allows the addition of another pertinent project information. The data also can be uploaded to a web-server for aggregation and customer reporting. In addition to a cable sensor, a new fiber optic cure verification (FCV)[93] has also been investigated to monitor the cure temperature continuously along the full length of a CIPP (cured-in-place pipe) liner. FCV uses laser pulsed over fiber optics to measure temperature continuously, eliminating the blind spots inherent in point measurement technologies. Both sensors can monitor the temperature changes of the curing process and also later during its service. However, in addition to temperature, other mechanical properties may also be of interest but not measured during the curing and service periods.

It should be noted that many municipalities take quality assurance (QA) samples or coupons for either laboratory testing or possible warranty claims. But these coupons may not be able to represent the actual conditions of the repaired pipes. Some assessments of CIPP lined pipes conducted by Environment Protection Administration (EPA) showed that for the sewer pipes rehabilitated using CIPP liners, 69% had defects and that CIPP liners had greater defect flow measurements after rehabilitation[94]. More in-situ monitoring techniques are in need for better assessment of the rehabilitated CIPP liners.

2.2.5 Finite Element Modeling of CIIP Liners

In addition to assessment and monitoring technologies, numerical analysis is also of great interest to study the performances of the CIPP liners. In this section, we reviewed the finite element modeling of CIPP liners in terms of mechanical performance and bonding performance between liner and pipeline.

Mechanical Performances: Three dimensional (3D) numerical model has been developed to investigate the mechanical properties of pipeline after CIPP rehabilitation under coupled effects of soil, traffic, and fluid loads[95, 96]. From the parametric study on the structural and fluid model, it showed that the cover depth and CIPP thickness had great effects on the corroded pipeline maximum principal stress and the CIPP von Mises stress, the traffic load had a great effect on the CIPP liner stress and pipe-liner composite vertical displacement, while fluid load had little effect on the pipe-liner composite structure. Among the whole pipeline, crown, invert, springline worth more attention. It was found that previous work had a drawback in analyzing the liner mechanical performance if the ratio of void diameter *d* to pipe inside diameter *D* exceeded one third[97]. Therefore, a 3D finite element isotropic analysis has been performed [97] on the CIPP liner spanning circular voids, as shown in Figure 12. The sensitivity study showed the axial bending stress took the place of hoop stress and became the governing stress in the liner as the ratio *d*/*D* close to unity. Besides, with the addition of the friction between the pipe and liner interface, the stress response was lower, and the friction coefficient of 0.36 was recommended. From the orthotropic analysis considering higher circumferential stiffness, hoop stress became the limiting factor for all void sizes[98], as shown in Figure 13. As the increase of the modulus ratio of hoop to axial, the axial stress decreased significantly while the hoop stress was stable. To reduce the maximum tensile stress, the hoop stiffness needs to be at least 1.1 times the axial modulus. In addition, the failure analysis can also be conducted based on the ASTM F2207-06 Standard Specification[99] and suggested a failure criterion for CIPP liner, shown in Equation (1) as:

$$\left(\frac{N_h}{(N_{uts})_h}\right)^2 - \frac{N_h N_a}{(N_{uts})_h^2} + \left(\frac{N_a}{(N_{uts})_a}\right)^2 = 1 \tag{1}$$

where N_h is the load/width in the hoop direction, N_a is the load/width in the axial direction, $(N_{uts})_h$ is the ultimate load/width in the hoop direction, and $(N_{uts})_a$ is the ultimate load/width in the axial direction. The structural failure occurred if either direction reached ultimate strength. The region beyond the overlap of two curves in Figure 14[98] indicated the failure area.

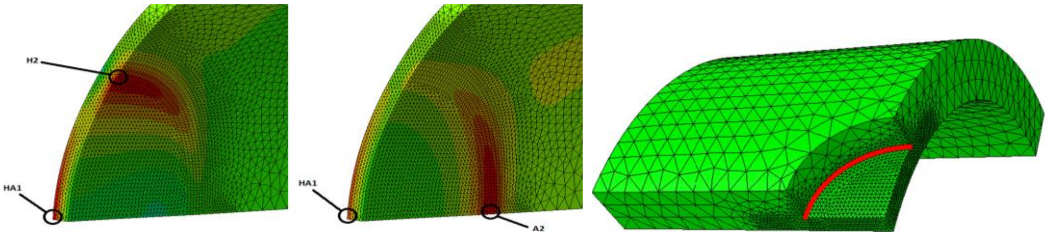

(a) (b)

Figure 12 (a) Contour plots of hoop stress and axial stress; (b) stress concentration at the sharp edge of the void[97].

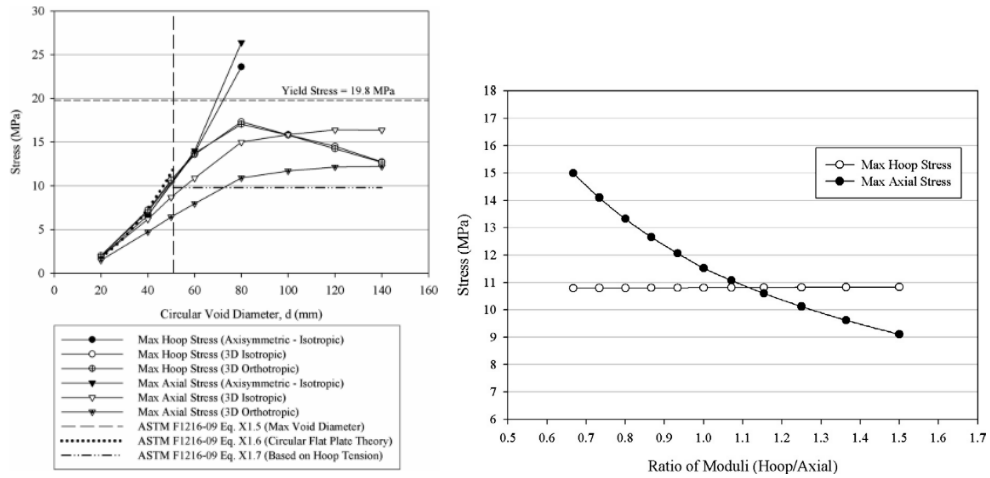

(a) (b)

Figure 13 (a) Maximum tensile hoop and axial stresses calculated from axisymmetric analysis and 3D orthotropic analysis; (b) the stress response versus ratio of moduli[98].

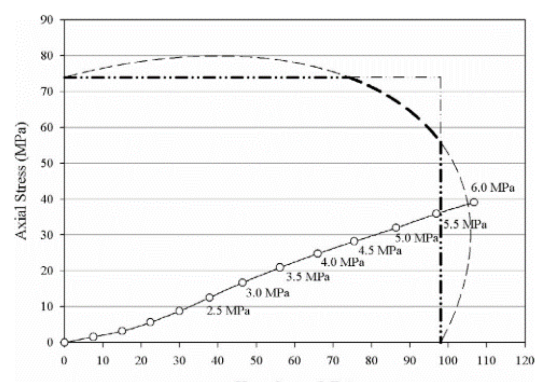

Figure 14 Graphical representation of the maximum and interactive stress criteria with load path curve of critical element[98].

Further finite element analysis (FEA)[100] were conducted on two urban aging gas pipelines with corrosion and perforation defects, repaired by inserted hose lining method. It concluded that inserted hose lining could effectively reduce the stress of the aging pipelines. The sensitivity study showed the maximum stress of the steel pipe and lining increased significantly from the decrease of residue pipe thickness, the increase of diameter, and the increase of in-pipe pressure, while the pipeline buried depth has little influence on the stress. Figure 15 shows the FEA results on the extreme condition of perforated pipe, where the risk of elliptical corrosion is slightly high than circular corrosion.

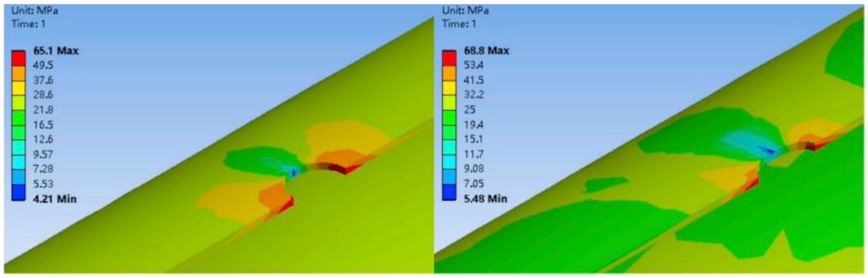

Figure 15 The stress contours of the steel pipeline with corrosion perforation after repair[100].

The performance of pipelines after CIPP rehabilitation were also analyzed through numerical methods[101], as shown in Figure 16. The blue part represented the real pavement, and yellow represented subgrade where liner buried in. The results showed the presence of CIPP significantly increased the pipe integrity and safety. The sensitivity study showed that the pipe corrosion width was inversely correlated with thickness of CIPP, while corrosion depth, traffic load, cover depth, and water quantity were positively correlated. In addition, the stress concentration at the CIPP due to the shear displacement caused by traffic should be minimized by balancing cover depth and CIPP thickness.

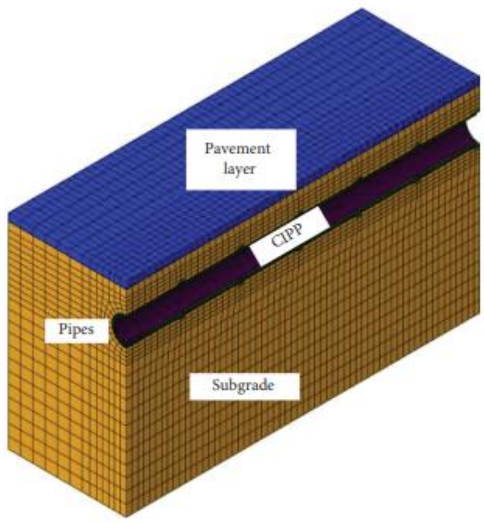

Figure 16 FEM 3D mesh geometry of CIPP rehabilitated pipe in subgrade[101].

The nonlinear composite liner also can be simulated as a homogenous material by curve fitting different materials' mechanical properties using ABAQUS[102]. The author conducted FEA to predict the liner condition during installation process. The highest stress was found at the bottom of liner after folding it. For pull-in-place installation, Figure 17[102] shows the prototype pipeline network. The pulling force was significant when passing the curve pipe. The relation between liner inflation and the number of wrap tapes was considered and validated. More wrap tapes require higher pressure to inflate the liner.

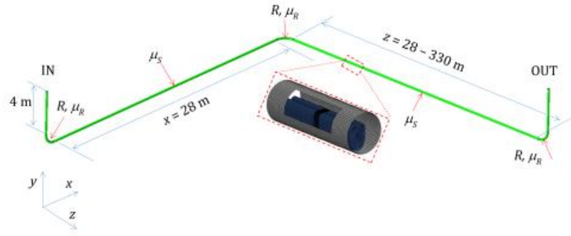

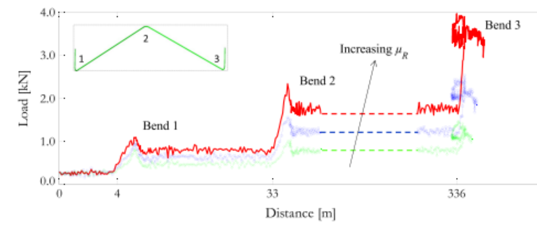

(a)

(b)

Figure 17 (a) Prototype pipeline network; (b) Load versus traveled distance with three different friction coefficients for pipe bends (red line represented the same coefficient for whole pipe) [102].

The CIPP lining method could potentially reduce stress concentration and displacement difference to consolidate the damaged pipe by numerical analysis and parametric study[103]. As shown in Figure 18, a circular area was used to simulate corrosion damage and different damage stages were analyzed by calculating void depth and radius. After installing CIPP, the pipe structural performance was reinforced with 45% and 70% reductions in stress and displacement[103]. It is found that the liner thickness had less effect on rehabilitation which was because the damage was not significant compared to the whole pipe and the lack of the consideration of liner bonding performance.

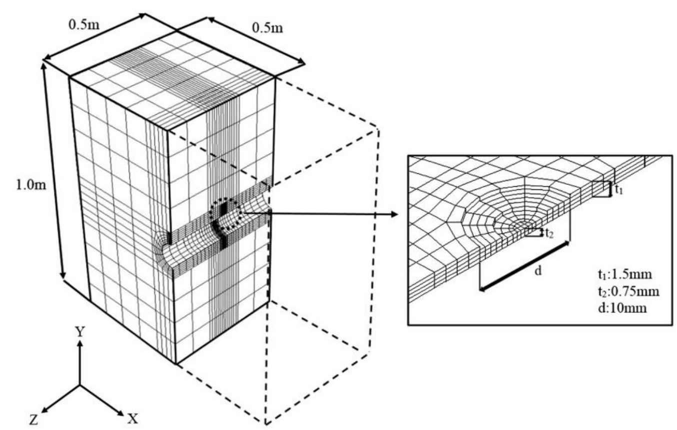

(a)

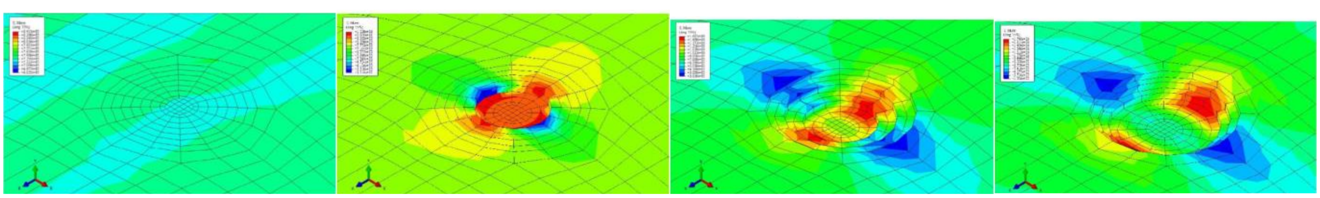

(b)

Figure 18 (a) The ABAQUS finite element mesh model with amplified corrosion area; (b) the stress history of the damage pipe, corroded with different void depth[103].

The elastic buckling behavior of polyhedral polymer structural liner was analyzed under external hydrostatic pressure through analytical method based on minimum potential energy and numerical methods based on finite element analysis[104], as shown in Figure 19. It was shown that the buckling pressure of a polyhedral liner increases with the increase of thickness-to-radius ratio and the decrease of the number of sides in polygon base shape. With the increase of ratio of thickness-to-radius, the improvement of structural liner critical stress decreased.

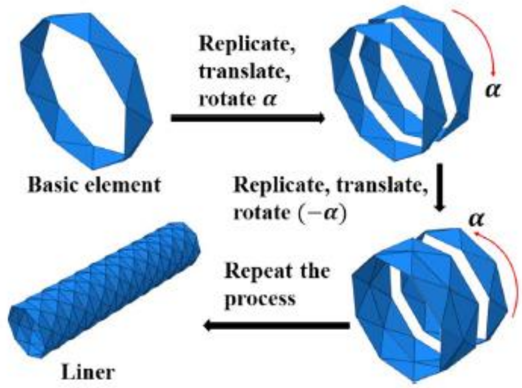

Figure 19 Formation of a polyhedral liner[104].

The finite element method (FEM) simulation for the buckling collapse of HDPE liners stated that deterioration of gas permeation would be worse expeditiously, which caused reduction in modulus and critical buckling pressure[105]. The imposed fluid flux was adopted in FEA to model the real pressure change. Figure 20 represented the buckling results of 3D HDPE liner model[105]. From the excellent agreement between the 2D and 3D models, a 2D model was executed the parametric study instead of 3D model to gain computational efficiency. The critical buckling stress was proved highly dependent of temperature, where higher temperature is detrimental.

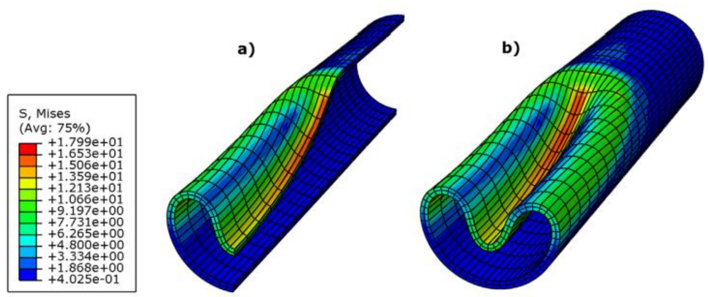

Figure 20 Von Misses stress contours of deformed geometry obtained by FEM simulation of the HDPE liner[105].

The effects of liner on the pipe with different patterns of cracks were also investigated using FEM[106]. A bias mesh was applied around the crack to capture the stress singularity with high fidelity. The author concluded that the circumferential crack had less effect on buckling strength than axial crack. With the increase of liner stiffness and thickness, the critical crack length increased. Figure 21[106] depicted the dependence of buckling mode shapes on the relative thickness and relative stiffness of the liner by examining the buckling load and crack orientation in global, local, and transition zone, which can be used to identify future failure types.

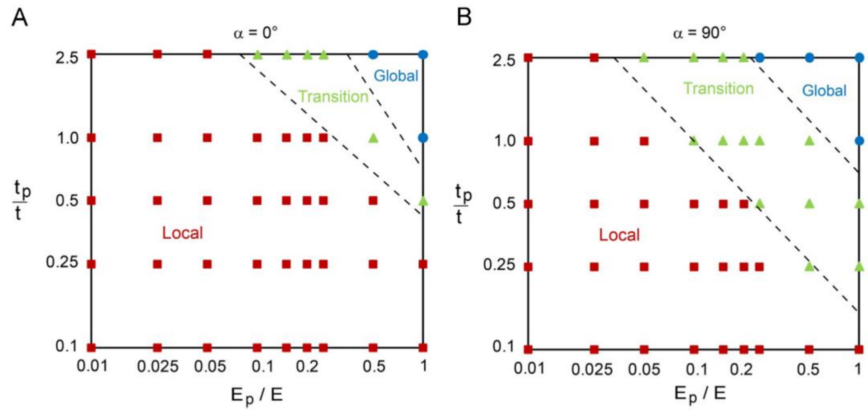

Figure 21 The maps showing the dominance of global, transitional and local buckling shapes in a lined cylindrical shell with a (A) circumferential and (B) longitudinal crack based on Young's modulus ratio, (Ep/E), and the thickness ratio, (tp/t)[106].

The liner buckling behavior with the variance of thickness was studied by FEM plane strain analysis[107]. A thinner section was assumed at the top due to gravity. The results in Figure 22 show that compared to uniform thickness pipe[107], the pipe with evenly decreased thickness (increasing m value) from bottom to top had a significantly low critical pressure. If the crown thickness is only half of the invert ($m = 0.5$), the buckling pressure dropped to a quarter compared with the perfect pipe ($m = 0$).

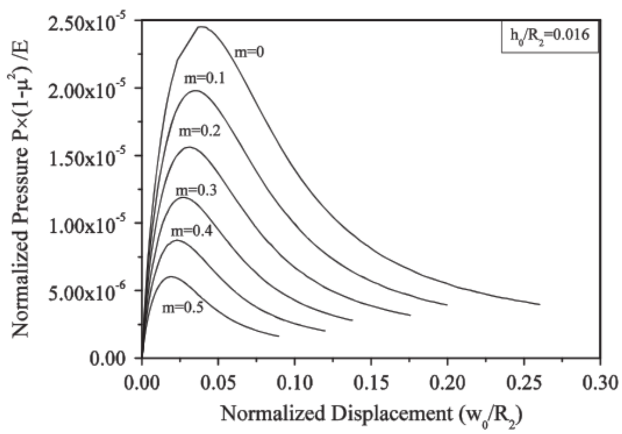

Figure 22 Pressure–displacement curves of elastic pipe linings with different thickness distribution[107].

When working under the high pressure, the polymer layer was easily to be penetrated by carbon dioxide and methane gases which increased the pressure in the interface and caused high potential of debonding or even radial buckling[108]. The hydrostatic elements were adopted to simulate the gap, as shown in Figure 23a. Compared with different material models, the elastoplastic with strain hardening model, shown in Figure 23b, was the most ideal one for all kinds of liner sizes[108].

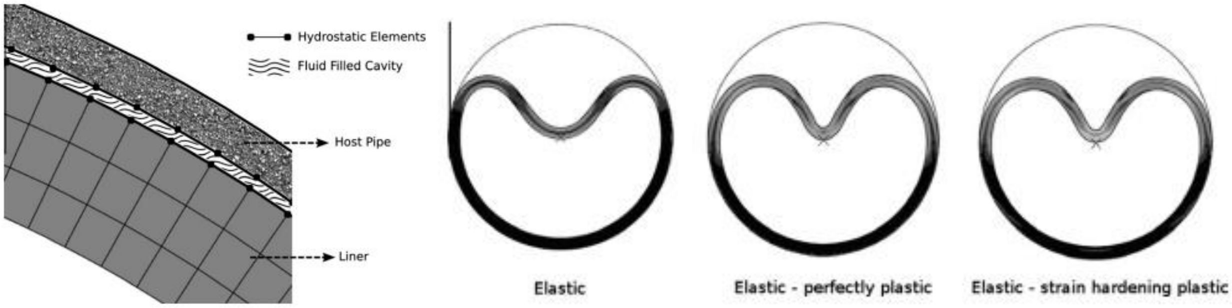

(a) (b)

Figure 23 (a) Cavity simulated with hydrostatic fluid elements. (b) Final collapse shapes for different material types[108].

A further numerical analysis studied the combined effect of pipe internal pressure and cover depth on CIPP liners, shown in Figure 24[109]. The reduction of stress values was observed when installed CFRP and GFRP liners as rehabilitation options.

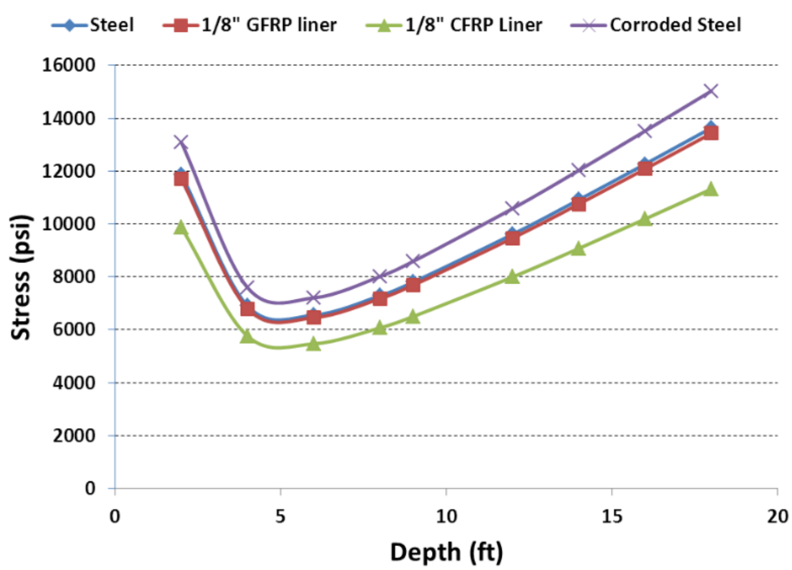

Figure 24 Liner stress versus buried depth[109].

Bonding Performances: For bonding performance, it is suggested to adopt cohesive elements in FEM to simulate adhesive bonding between substrate and liner[110]. In addition, a calculation method based on damage weight distribution was proposed to estimate the structural damage. The wellbore pressure is the major factor induced the liner interfacial bond detachment and other structural failures[111]. Besides, the higher axial stress was observed along liner with at lower possion's ratio which may affect interfacial bonding performance. The debonding occurred between liner and pipeline if the pipe was depressurized suddenly from repair or maintenance through FEA and field test, shown in Figure 25a[111]. This phenomenon could be more severe if the pipeline experienced depressurization cycles. It was assumed in the FEA that certain gas was trapped in a void between liner and pipe without considering the gas diffusion mechanism. Cohesive zone model was adopted to monitor the adhesive behavior and interfacial failure. With the increase of initial pipe pressure, adhesive strength, void size and/or the decrease the liner tensile modulus, the disbondment would be more severe. In addition, implementation of liner in bended pipe was considered in the lab tests. Debonding was observed after depressurization at the bend, as shown in Figure 25b[111]. More attention should be paid to the attachment condition around the curve pipe.

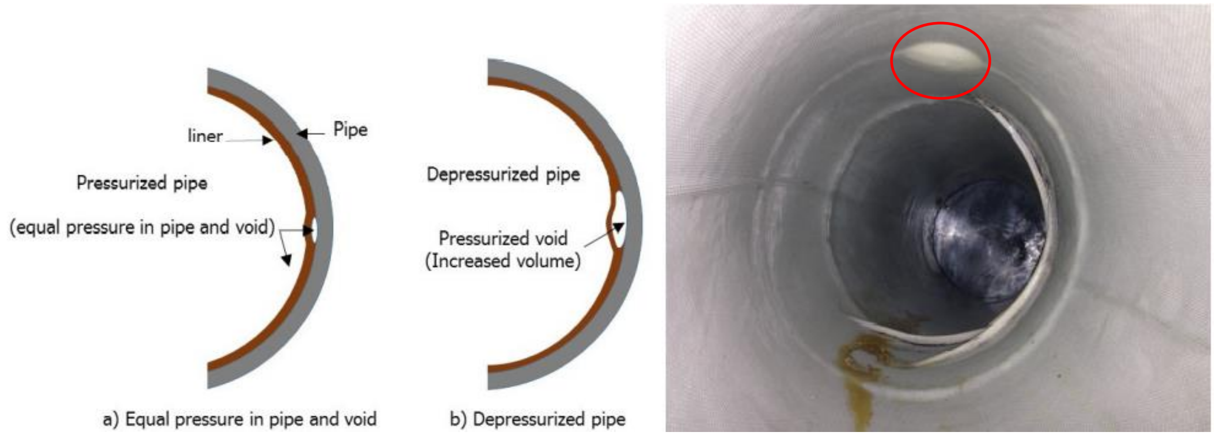

(a)

(b)

Figure 25 (a) Diagram of void expansion after depressurization; (b) small detachment at the top after depressurization[111].

The FEA is also suitable for analyzing the stress level of liner with inadequate bonding[112, 113]. In the earlier study, the effect of liner geometry and imperfections on buckling behavior was simulated with FEA. Figure 26 showed among three imperfection types, local and loose-fitting imperfection had the higher potential of buckling failure[112, 113]. The author stated the critical pressure decreased significantly as the increase of imperfection amplitude Δ_0 and gap size d. FEA was recommended to evaluate the critical stress of the liner fitted in the pipe with a new formulation of the enhancement factor to evaluate the critical stress of encased liner.

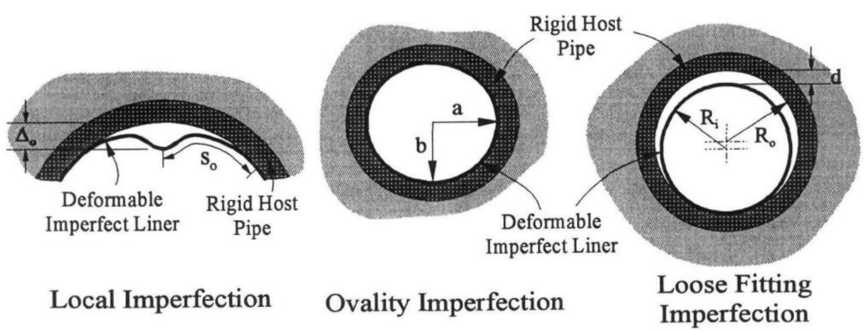

Figure 26. Different Types of Liner Imperfection[112].

2.2.6 Risk Analysis of Pipelines and Liners

The data obtained from all the material testing, property assessments, and numerical analysis can be beneficial to the management of the CIPP liners and the corresponding rehabilitated pipelines through risk analysis. In this section, we reviewed the risk assessment methods in ASME pipeline standard, stochastic/probabilistic approaches, and machine learning-based approaches. We also reviewed different types of risk in the pipelines in terms of the pipe failure effect, construction & in-service risk, and environmental risk.

ASME Pipeline Risk Assessment: According to ASME standard[114], the pipeline integrity management process should follow seven steps which guide the data collection and risk assessment, including:

(a) Identify Potential Pipeline Impact by Threat: ASME classify the pipeline integrity threat in 22 root causes. One of the 22 causes is “unknown” based on operator’s report. The others are divided in to 9 categories, including external corrosion, internal corrosion, stress corrosion cracking, manufacturing-related defects, welding/fabrication related, equipment, third-party/mechanical damage, incorrect operational procedure, and weather-related and outside force[114].

(b) Gathering, Reviewing, and Integrating Data: For data gathering, the limited data sets shall be gathered to evaluate each threat for prescriptive integrity management program applications, as shown in Table 2[114]. The data needed for integrity management programs can be obtained from within the operating company and from external sources (e.g., industry-wide data). Besides, existing management information system (MIS) or geographic information system (GIS) databases and the results of any prior risk or threat assessments are also useful data sources. The data sources listed in Table 3 are necessary for integrity management program initiation[114].

Table 2 Data Elements for Prescriptive Pipeline Integrity Program[114]

Category	Data
Attribute data	Pipe wall thickness
	Diameter
	Seam type and joint factor
	Manufacturer
	Manufacturing date
	Material properties
	Equipment properties
Construction	Year of installation
	Bending method
	Joining method, process and inspection results
	Depth of cover
	Crossings/casings
	Pressure test
	Field coating methods
	Soil, backfill
	Inspection reports
	Cathodic protection (CP) installed
	Coating type
Operational	Gas quality
	Flow rate
	Normal maximum and minimum operating pressures
	Leak/failure history
	Coating condition
	CP system performance
	Pipe wall temperature
	Pipe inspection reports
	OD/ID corrosion monitoring
	Pressure fluctuations
	Regulator/relief performance
	Encroachments
	Repairs
	Vandalism
	External forces

Inspection	Pressure tests In-line inspections Geometry tool inspections Bell hole inspections CP inspections (CIS) Coating condition inspections (DCVG) Audits and reviews

Table 3 Typical Data Sources for Pipeline Integrity Program[114]

Process and instrumentation drawings (P&ID)
Pipeline alignment drawings
Original construction inspector notes/records
Pipeline aerial photography
Facility drawings/maps
As-built drawings
Material certifications
Survey reports/drawings
Safety-related condition reports
Operator standards/specifications
Industry standards/specifications
O&M procedures
Emergency response plans
Inspection records
Test reports/records
Incident reports
Compliance records
Design/engineering reports
Technical evaluations
Manufacturer equipment data

(c) Risk Assessment: For risk assessment, both prescriptive-based and performance-based integrity management programs are required. Risk is typically described as the product of two primary factors: the failure likelihood (or probability) that some adverse event will occur and the resulting consequences of that event. Method to describe the risk depending on the pipeline integrity classification is shown as follows[114]:

$$\text{Risk}_i = P_i \times C_i \text{ for a single threat,} \tag{1}$$

$$\text{Risk} = \sum_{i=0}^{9} (P_i \times C_i) \text{ for threat categories 1 to 9,} \tag{2}$$

$$\text{Total segment risk} = (P_1 \times C_2) + P_2 \times C_2 + \cdots + P_9 \times C_9. \tag{3}$$

where the failure threat category is from 1 to 9, *C* is the failure consequence, and *P* is the failure likelihood.

In order to conduct risk assessment for pipeline segment, a risk priority shall be established at first. Then one or more risk assessment methods are applied to estimate the risk. ASME lists four risk assessment methods: Subject Matter Experts (SMEs), Relative Assessment Models, Scenario-Based Models, and Probabilistic Models. SMEs combine the information from operating company or consultants and technical literatures, and then assign the relative likelihood and consequence value to calculate the risk. Relative assessment models are based on more extensive data. Models that identify and quantitatively weigh the major threats and consequences relevant to past pipeline operations are used. Scenario-Based Models create models that generate a description of an event or series of events leading to a level of risk and includes both the likelihood and consequences of such events. Probabilistic models have the highest data requirements. The risk output is provided in a format that is compared to acceptable risk probabilities established by the operator, rather than using a comparative basis.

Risk analysis includes two parts, which are the Prescriptive Integrity Management Programs and Performance-Based Integrity Management Programs. For Prescriptive Integrity analysis, the reinspection interval of pipeline segment integrity assessment is based on Table 4[114]. MAOP means pipeline segment's maximum allowable operating pressure, psig (kPa). For Performance-Based Integrity analysis, performance-based integrity management programs shall prioritize initial integrity assessments utilizing any of the methods (four risk assessment methods mentioned before). Based on the above two parts, the following general characteristics should be considered: Attributes, Resources, Operating/Mitigation History, Predictive Capability, Risk Confidence, Feedback, Documentation, "What If" Determinations, Weighting Factors, Structure, Segmentation.

(d) Integrity Assessment: After gathering the data and completing the risk assessment for each threat and for each pipeline segment or system, an appropriate integrity assessment method shall be identified for each pipeline system or segment. ASME also lists four integrity assessment methods of pipeline. They are In-line inspection (ILI), Pressure testing, Direct Assessment, and Other Integrity Assessment Methodologies. For prescriptive-based integrity management programs, the alternative integrity assessment shall be an industry-recognized methodology.

(e) Responses to Integrity Assessment, Mitigation (Repair and Prevention), and Setting Inspection Intervals: After the integrity assessment, it is required to take measures to mitigate the impact based on the response to the integrity assessment.

(f) Update, Integrate, and Review Data: After doing initial integrity assessments, the updated information shall be retained and added to the database of information used to support future risk assessments and integrity assessments.

(g) Reassess Risk: Risk assessment shall be performed periodically within regular intervals and when substantial changes occur to the pipeline.

Table 4 Integrity Assessment Intervals: Time-Dependent Threats, Internal and External Corrosion, Prescriptive Integrity Management Plan[114]

Inspection Technique	Interval, yr [Note (1)]	Criteria: Operating Pressure Above 50% of SMYS	Operating Pressure Above 30% But Not Exceeding 50% of SMYS	Operating Pressure Not Exceeding 30% of SMYS
Hydrostatic testing	5	TP to 1.25 times MAOP [Note (2)]	TP to 1.39 times MAOP [Note (2)]	TP to 1.65 times MAOP [Note (2)]]
	10	TP to 1.39 times MAOP [Note (2)]	TP to 1.65 times MAOP [Note (2)]	TP to 2.20 times MAOP [Note (2)]
	15	Not allowed	TP to 2.00 times MAOP [Note (2)]	TP to 2.75 times MAOP [Note (2)]
	20	Not allowed	Not allowed	TP to 3.33 times MAOP [Note (2)]
In-line inspection	5	P_f above 1.25 times MAOP [Note (3)]	P_f above 1.39 times MAOP [Note (3)]	P_f above 1.65 times MAOP [Note (3)]
	10	P_f above 1.39 times MAOP [Note (3)]	P_f above 1.65 times MAOP [Note (3)]	P_f above 2.20 times MAOP [Note (3)]
	15	Not allowed	P_f above 2.00 times MAOP [Note (3)]	P_f above 2.75 times MAOP [Note (3)]
	20	Not allowed	Not allowed	P_f above 3.33 times MAOP [Note (3)]
Direct assessment	5	All immediate indications plus one scheduled [Note (4)]	All immediate indications plus one scheduled [Note (4)]	All immediate indications plus one scheduled [Note (4)]
	10	All immediate indications plus all scheduled [Note (4)]	All immediate indications plus more than half of scheduled [Note (4)]	All immediate indications plus one scheduled [Note (4)]
	15	Not allowed	All immediate indications plus all scheduled [Note (4)]	All immediate indications plus more than half of scheduled [Note (4)]
	20	Not allowed	Not allowed	All immediate indications plus all scheduled [Note (4)]

NOTES:

(1) Intervals are maximum and may be less, depending on repairs made and prevention activities instituted. In addition, certain threats can be extremely aggressive and may significantly reduce the interval between inspections. Occurrence of a time-dependent failure requires immediate reassessment of the interval.

(2) TP is test pressure.

(3) P_f is predicted failure pressure as determined from ASME B31G or equivalent.

(4) For the direct assessment process, indications for inspection are classified and prioritized using NACE SP0204, Stress Corrosion Cracking (SCC) Direct Assessment Methodology; NACE SP0206, Internal Corrosion Direct Assessment Methodology for Pipelines Carrying Normally Dry Natural Gas (DG-ICDA); or NACE SP0502, Pipeline External Corrosion Direct Assessment Methodology. The indications are process-based and may not align with each other. For example, the External Corrosion DA indications may not be at the same location as the Internal Corrosion DA indications.

Stochastic/probabilistic Approaches: Stochastic approaches also have been investigated for risk analysis, such as the use of the Artificial Neural Network-Based Models (ANN) and fuzzy inference system (FIS) to predict the risk index[115]. In the model, the FIS model was used in the first part to consider 8 main causes and 30 root cause, as shown in Figure 27, and select their probability based on Matlab fuzzy toolbox. In the second part, ANN model is chosen based on the best performance model by providing the lowest MSE and highest R2, and the final choice is shown in Figure 28[115].

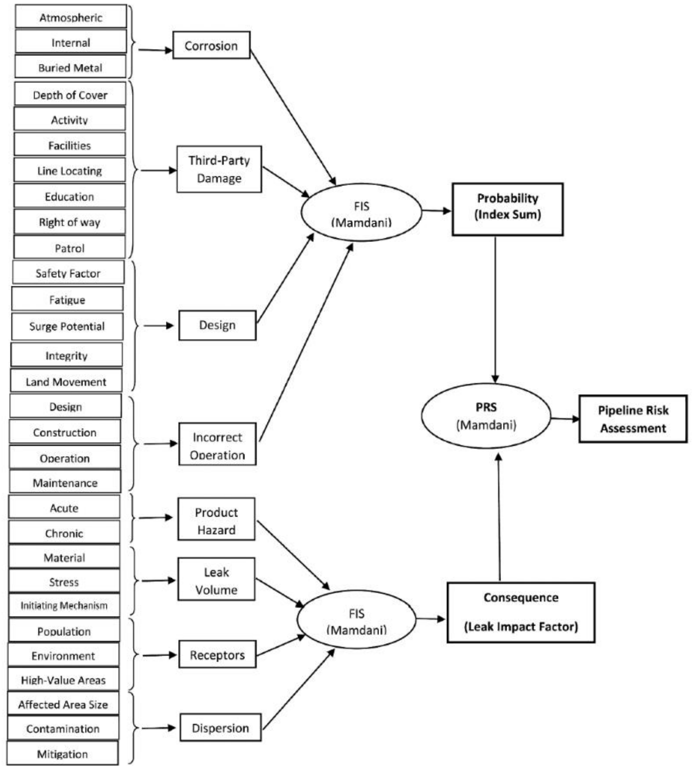

Figure 27 FIS-ANN risk assessment model[115].

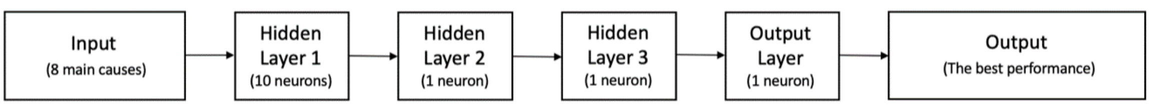

Figure 28 The structure of the selected ANN[115].

The Fuzzy Bayesian Networks (FBN) model was investigated for safety risk analysis in tunnel construction. The detailed procedures are shown in Figure 29[116]. In the FBN model, the authors predicted the probability of factors based on the Equation (4)-(6) as:

$$P_i = \sum_{i=1}^{S} \frac{P_i}{S}, \tag{4}$$

$$m = E(P) = \sum_{i=1}^{9} (C_i \times P_i), \tag{5}$$

$$\sigma = \sqrt{D(P)} = \sqrt{\sum_{i=1}^{9} \left[\left(C_i - E(P) \right)^2 \times P_i \right]}. \tag{6}$$

where $a = m - 3$, $b = m + 3C_i$ refers to the mean of the i^{th} probability interval, a, m and b refer to the characteristic values of a triangular fuzzy number. In the case study, factors including poor geological conditions, unreasonable design parameters, poor construction quality, and improper management were considered.

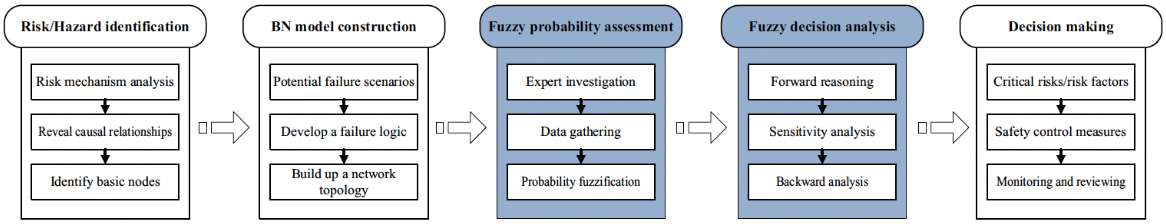

Figure 29 A FBN-based decision approach with detailed step-by-step procedures[116].

A Bayesian Network (BN) model was also applied to access pipeline safety caused by third-party damage (TPD) based on Bayesian theory[117]. In this model, the authors mainly considered three influencing factors: machinery hits, strength of pipeline, and geological disasters. Accordingly, a failure model was promoted to evaluate failure probability of an oil and gas pipeline[118]. In this model, the authors applied Monte Carlo simulation and First Order Second Moment (FOSM) method that includes characterization of defect geometry, internal corrosion growth rate, and remaining mechanical hoop strength capacity, shown in Equations (7-10) as[118]:

$$g(X) = d_c - d, \tag{7}$$

$$\beta = \frac{\mu_{d_c} - \mu_d}{\sqrt{{\sigma_{d_c}}^2 + {\sigma_d}^2}}, \tag{8}$$

$$P_f = \varphi(-\beta) = 1 - \varphi(\beta), \tag{9}$$

$$R = P_f \times C. \tag{10}$$

where d_c is critical defect depth which is 80% of wall thickness (t), d is the defect depth, β is reliability index, P_f is the failure probability, C is the consequence which is known for a specific material and specific location, and R is the risk.

A reliability assessment model was developed by using Non-homogeneous Poisson process (NHPP) to evaluate normal and defective states of oil pipeline[119]. This model used the delay time concept to find some defect signals and the factors considered are corrosion process and shock damages. In addition, an oil & gas pipeline internal corrosion risk assessment was proposed by using Bayesian belief network[120]. This study combined different corrosion models such as general corrosion model, pitting corrosion and erosion-corrosion models, microbiologically influenced corrosion (MIC) model and corrosion defect model to predict probability of failure. Though sensitivity analysis, operating pressure (OP) and defect depth (DD) are the two most influential parameters. The other input nodes are shown in Figure 30. The inputs also incorporated the composition of the fluid passing through the pipe.

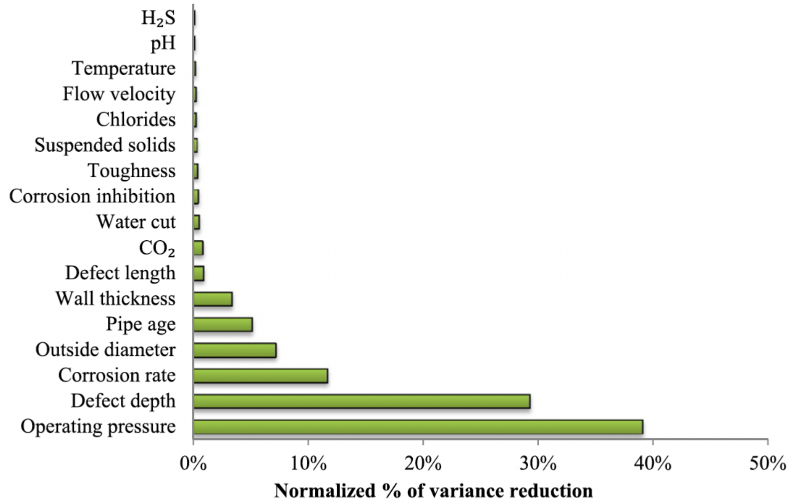

Figure 30 Sensitivity analysis of the Pipe Failure (PF) node based on variation in the input nodes[120].

The Fuzzy Bayesian Network with a Bow-Tie model was also investigated to conduct risk analysis for gas pipeline[121]. In the model, the leakage of natural gas was considered as the primary event and studied two kinds of factors for pipeline failure: external factors and internal factors. Details are shown in Table 5[121]. The other part of Bow-Tie model is the consequence of the event tree (Table 6[121]). Equations (11) and (12) are applied to obtain the failure probability from fuzzy probability, which translated experts' linguistic comments into data results as[121]:

$$P = \begin{cases} \frac{1}{10^Z} & P^* \neq 0 \\ 0 & P^* = 0 \end{cases}, \tag{11}$$

where

$$Z = 2.301 \left(\frac{1 - P^*}{P^*}\right)^{\frac{1}{3}}. \tag{12}$$

Another fuzzy Bayesian belief network model was also used to access the risk of oil and gas pipeline[122]. Though sensitivity analysis, construction defect, overload, mechanical damage, bad installation, and quality of worker have more effect on pipeline safety. The probabilities and 66 different considered factors are shown in Table 7[122].

Table 5 The natural gas leakage[121]

Primary event	Potential factors	Details
leakage failure of pipelines	external factors	corrosion
		interference from third party
		natural disaster
	internal factors	material defect
		weld-seam defect
		auxiliaries failure

Table 6 Consequence of the event tree

No.	Consequence
A1	Detonation or deflagration
A2	Fireball or jet fire
A3	Confined vapor cloud explosion
A4	Flash fire
B1	Severe casualties
B2	Light casualties
B3	No casualties
C1	Severe poisoning and contamination
C2	Light poisoning and contamination
C3	Material loss

Table 7 Posterior probabilities of the parent and child nodes after updating[122]

	Probabilities			Probabilities	
Parent nodes	Posterior	Increase	Child nodes	Posterior	Increase
Apparatus	.0548	.0003	Pipe failure	1.0000	.5655
Bacteria	.1371	.0006	Puncture	.2657	.1502
Bad Groove	.0299	.0169	Rupture	1.0000	.5655
Bad Installation	.2510	.1690	Acid Medium	.3418	.0224
Bad Microstructure	.0485	.0235	Alternative Stress	.0343	.0020
Bad Weld	.1595	.0420	Corrosion	.1866	.0490
CO_2	.0626	.0041	Corrosion Fatigue	.0052	.0030
Coarse Grain	.0665	.0250	Corrosion Medium	.2761	.1561
Construction Defect	.1955	.1080	Corrosion Thinning	.0795	.0450
Debonding	.1321	.0076	Defect of Pipe	.2928	.2190
Earthquake	.0306	.0173	External Corrosion	.2530	.1430
Electrical Interference	.3204	.0014	Geological Hazard	.0713	.0403
Equipment	.1151	.0836	Incorrect Operation	.3991	.2257
External Load	.0439	.0214	Inference from Third party	.3758	.2125
Failure of CP	.2183	.0133	Initial Defect	.0918	.0519
Failure of Coating	.1423	.0603	Internal Corrosion	.0512	.0289
Failure of Inhibitor	.1565	.0090	Maintenance	.2634	.1445
Flood	.0519	.0224	Material Defect	.2737	.1189
H_2S	.1204	.0079	Operation	.2737	.1548
High Salt	.1261	.0006	Operational Defect	.2762	.1200
High Temperature	.2526	.0011	Protection Measure	.3456	.0307
High Water Ratio	.1783	.0008	SCC	.0052	.0030
Implicit Signage	.0311	.0176	Soil Corrosion	.2532	.1100
Large Internal Stress	.0833	.0308	Tensile Stress	.0341	.0020
Low Resistance	.2195	.0010	Unreasonable Design	.0990	.0560
Low pH	.1997	.0807			
Mechanical Damage	.1750	.0900			
Metal Contamination	.0519	.0124			
O_2	.1985	.0130			
Overload	.2532	.1432			
Parties Ignore Signage	.0718	.0293			
Pressure Surge	.0406	.0106			
Quality of Worker	.2762	.1562			
Residual Stress	.0496	.0106			
SCADA	.0430	.0180			
Sabotage	.0322	.0182			
Stress Concentration	.1017	.0167			
Subsidence	.0896	.0211			
Unreasonable Strength	.0683	.0273			
Unsuitable Material	.1518	.0943			
With Water	.2467	.0257			

Machine Learning-based Approaches: Machine Learning (ML) methods have also been explored for analyzing pipeline risks. Among various ML methods, the k-means and Gaussian mixture model (GMM) was developed to classify different corrosivity level clusters and established a clustering-based approach to assess the soil corrosivity for external integrity management of a pipeline structure[123] and a failure model combining regression analysis and artificial neural networks (ANNs) model was developed to predict the oil pipeline failure[124]. These models applied Equation (13) to conduct the regression analysis and consider five factors: type of product, pipe location, pipe age, land use, and pipe diameter. In the ANN model component, the authors considered one hidden layer, as shown in Figure 31[124].

$$Y_i = \beta_0 + \beta_1 X_{i1} + \beta_2 X_{i2} + \cdots + \beta_{p-1} X_{ip-1} + \varepsilon_i \tag{13}$$

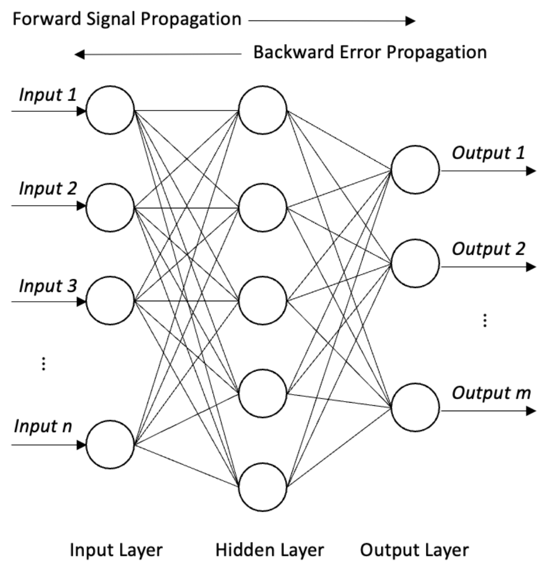

Figure 31 Schematic architecture of ANN with one hidden layer (adopted from Al-Barqawi and Zayed, 2008)[124]

The fuzzy inference system (FIS) was applied to establish a risk index model[125]. Factors considered in the model are shown in Figure 32. The Crystal Ball-Monte Carlo simulation was used to examine the factors and analyze sensitivity for the risk index model, considering the reflect satisfactory values such as the coefficient of variation and mean standard error. Later, a data-driven-model (DDM) was proposed combining the simulation and regression algorithms to predict water pipeline failure[126]. The factors considered included water pressure and flow velocity. In the model, the authors applied the machine learning toolbox of MATLAB © R2019b to define the polynomial functions and choose the best DDM depending on R-square (R2), adjusted R-square (Adj R2), the sum of squares due to error (SSE), and root mean squared error (RMSE). The polynomial functions (first-order, second-order and third-order) are shown from Equation (14) to (16)[126]:

$$y = 0.9932x - 22.89, \tag{14}$$

$$y = 0.00098x^2 + 0.94x - 22, \tag{15}$$

$$y = -0.0055x^3 + 0.47x^2 - 13x + 110. \tag{16}$$

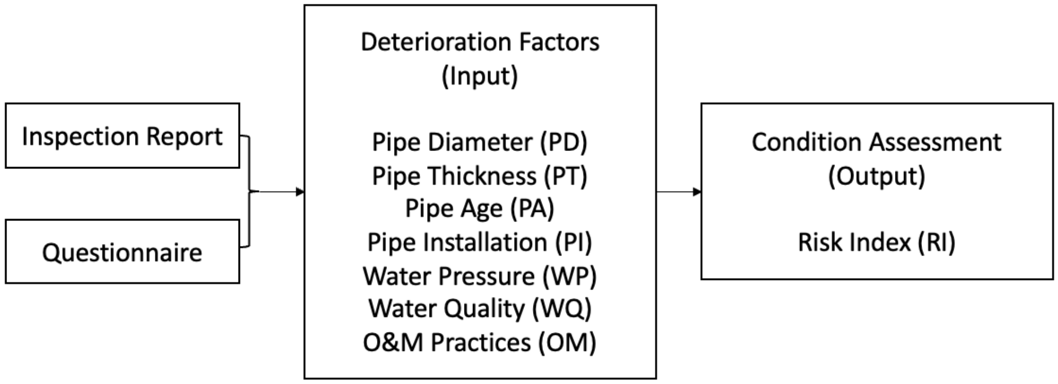

Figure 32 Inputs and output of the model[125].

In addition, multiple neural networks and fuzzy logic system was also investigated to establish pipeline assessment model, as shown in Figure 33[127]. In the model, the authors applied feature pattern recognition to input features such as pipeline length, angle, area to detect cracks, and service laterals.

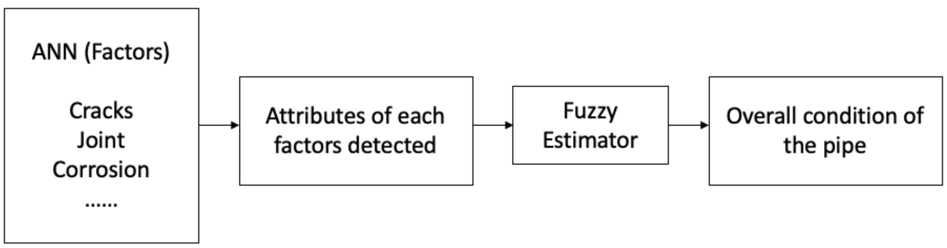

Figure 33 Fuzzy Approach for Rating of Defects[127].

A pipeline leakage model was investigated l[128] using the bow-tie model to build the relationship between pipeline leakage and possible accident and then used Bayesian network model to overcome the difficulties of bow-tie in modeling uncertainties and conditional dependency. The fault tree method was applied to show the factors corrosion, external loads, suspended span, natural disaster, material defect, weld-seam defect and auxiliaries failure. Accordingly, risk assessment software (ALOHA) and geography information systems (SuperGIS and Surfer) was used to predict the pipeline leakage[129] which used a simplified risk value (SRV) as shown in Equation (17), which considered the factors the potential effects of vapor diffusion, thermal radiation from combustion, and overpressure from an explosion as[129]:

$$SRV = hazard\ radius \times frequency. \tag{17}$$

where the hazard radius was measured in kilometers and the frequency was defined as the number of occurrences per year.

For water pipelines, a specific water pipeline leakage model was developed by combining machine learning and wireless sensors networks[130], using Support Vector Machine (SVM) as a classifier to identify the leaks, and applying the time-frequency analysis method to get complexity from approximate entropy (ApEn) to identify pipeline leakage. The non-linear regression analysis was also studied to establish the pipe failure rate equation, as shown in Equation (18) [131]. This equation considered pipe age and diameter to describe the pipe failure rate as:

$$F_r = 0.109 \cdot \exp(-0.0064 \cdot D_i) \cdot y_{age}^{1.377}. \tag{18}$$

where F_r is failure rate(breaks/km/year), D_i is the pipe diameter (mm), and Y_{age} is the pipe age (year).

Types of Risk: There are three types of risks including pipe failure effects, construction risk, in-service risk, and environmental risks. For pipe failure effects, the pipelines are easy damaged by chemistry reasons [132]. The factors change in tensile strength, elongation, weight loss or gain, crystallinity, chemical properties, and molecular structure are important to pipeline risk assessment. The risk models usually considered pipe age, pipe diameter, pipe wall thickness, type of product, operating pressure, history and causes of any releases, proximity to populated areas or environmentally sensitive areas, and the findings of prior tests and inspections, as the influencing factors[133].

For the construction risk and in-service risk, a pipeline risk level evaluation based on the risk of landslides can be used that may occur during the construction of pipeline projects[134] using a risk index R, which represented the risk of landslide induced by the construction of pipeline as [133]:

$$R = \sum_{i=0}^{m} W_i f_i(x) . \tag{19}$$

where m is total number of disaster assessment indicators, W_i is the weight coefficient of the ith evaluation index, $f_i(x)$ is the characteristic value of the index of the ith evaluation index. The risk grade used in this study can be seen in Table 8.

Table 8 Risk Grade[134]

Risk Grade	R
Low risk	Less than 0.22
Lower risk	0.22 – 0.34
Middle risk	0.34 – 0.46
Higher risk	0.46 – 0.58
High risk	More than 0.58

For the environmental risk, Table9 lists the potential environmental risk index during for pipeline construction[134].

Table 9 Environmental Geological Disasters Risk Index System[134]

Evaluation index	Target factors	Influence coefficient
Rainfall	Annual rainfall < 350 mm/a	0.5
	Annual rainfall = 350–400 mm/a	0.7
	Annual rainfall > 400 mm/a	0.9
River degradation	Convex bank	0.1
	Vertical bank	0.2
	Concave bank	0.4
Terrain slope	0–10°	0.1
	10–25°	0.4

	25–40°	0.8
	40–60°	0.5
	60–90°	0.5
Formation lithology	Soil	0.6
	Rock	0.1
	Tatter rubble	0.2
Engineering activities	Weak	0.1
	Relatively weak	0.2
	Relatively strong	0.4
	Strong	0.7
	Particularly strong	1.0
Control measures	Antislide retaining wall	0.5
	Antislide pile	0.4
	Anchor retaining wall	0.3
	Framed anchor	0.2
Construction season	Rainy season	0.7
	Nonrainy season	0.3

2.3 Student Mentoring

During the first quarter, six graduate students (Tofatun Jannet, Ph. D. student from NDSU, Loenard Chia, Ph.D. student from NDSU, Yasir Mahmood, Ph. D. student from NDSU, Austin Knight, Ph. D. student from NDSU, Junyi Duan, Ph. D. student from Purdue, Xiaoyue Zhang, Ph. D. student from Purdue) and one undergraduate research assistant (Colby Rance, sophomore student from NDSU) were hired to work on this project. All six graduate students completed their hiring process and will start their contracts on this project in the first week of January 2023. These students will continue working on this project from Quarter 2 to Quarter 3.

2.4 Outreach Activities

On Oct. 25th, 2022 (8 am to 2 pm), an one-day outreach event named “Pipeline Challenge” workshop in BrainSTEM was conducted based on this project. This workshop intended to let the middle school students have hands-on experiences using easy tools to plan and build pipeline. It is expected to encourage and generate interests for young kids to pursue pipeline engineering for future college education or careers. Table 10 is the schedule of the event. The “Pipeline Challenge” workshop contributed to all three sessions of the BrianSTEM program, with around 20 students in each session. Approximately 60 middle school students attended this workshop. Two graduate students volunteered in this outreach event to guide the middle school students. Figure 34 shows the photos taken from this event. More outreach events are planned for elementary school students in next quarter.

Table 10 Outreach BrainSTEM Workshop Schedule

8:00	-	9:00	Presenter Arrival
9:00	-	9:25	Student Arrival
9:25	-	9:40	Welcome
9:50	-	10:40	Session 1
10:50	-	11:40	Session 2
11:45	-	12:25	Lunch
12:30	-	1:20	Session 3
1:20	-	1:30	Students board buses

Figure 34 Photos of the BrainSTEM outreach events

3. Future work

In the second quarter, there will be three objectives:

1) Focus on the research activities planned in Tasks 2.1 and 3.1;
2) Supervise the graduate and undergraduate students in performing research Tasks 2.1 and 3.1;
3) Conduct an outreach workshop series for elementary school students.

References

1. Farrag, K., Evaluation of Structural Liners for the Rehabilitation of Liquid and Natural Gas Piping Systems, PHMSA: DTPH56-13-T-000012. 2015.
2. Primus Liner Product Specfications, Linears by Primus Line®. https://www.primusline.com/en/product/liner.
3. Bethel, K.; Catha, S. C.; Kanninen, M. F.; Stonesifer, R. B.; Charbonneau, K.; Ekelund, A.; Mandich, I.; McIntosh, R.; Stringfellow, W. D., The Design, Development and Validation of an Innovative High Strength, Self Monitoring, Composite Pipe Liner for the Restoration of Energy Transmission Pipelines. International Pipeline Conference 2006, 551-560.
4. Fiberspar Pipeline, Engineering Guide, Section 1.2. www.fiberspar.com.
5. The Starline Trenchless Technology. http://www.starlinett.com/products/frame_cip.html.
6. GTI, Review and Selection Guide for Pipe Rehabilitation, GTI Project No. 20674, Operations Technology and Development (OTD). 2009.

7. Fu, G.; Shannon, B.; Rathnayka, S.; Deo, R.; Kodikara, J. State of The Art Literature Review on CIPP liners; CRC Project: Smart Linings for Pipe and Infrastructure, 2020.

8. Stewart, H. E.; O'Rourke, T. D.; Wham, B. P.; Netravali, A. N.; Argyrou, C.; Zeng, X.; Bond, T. K. Performance Testing of Field-Aged Cured-in-Place Liners (CIPL) for Cast Iron Piping; Final report to NYSEARCH/Northeast Gas Association, 2015.

9. Allouche, E.; Bainbridge, K.; Moore, I., Laboratory examination of a cured in place pressure pipe liner for potable water distribution system. 2005.

10. Downey, D.; Heavens, J.; Ngo, S., Principles and Practice for the Design and Selection of Pressure Pipe Lining Systems, Annual Technical Conference of the North American Society for Trenchless Technology. 2007.

11. Alam, S. Z. Experimental and Numerical Evaluation of Cured in Place Pipe Lining System for High Temperature Applications in Sewer Pipes. Doctoral dissertation, Louisiana Tech University, 2011.

12. Liu, T.; Zhao, B.; Zhang, J., Recent development of repairable, malleable and recyclable thermosetting polymers through dynamic transesterification. Polymer 2020, 194, 122392.

13. Denissen, W.; Droesbeke, M.; Nicolaÿ, R.; Leibler, L.; Winne, J. M.; Du Prez, F. E., Chemical control of the viscoelastic properties of vinylogous urethane vitrimers. Nature Communications 2017, 8 (1), 14857.

14. Capelot, M.; Montarnal, D.; Tournilhac, F.; Leibler, L., Metal-Catalyzed Transesterification for Healing and Assembling of Thermosets. Journal of the American Chemical Society 2012, 134 (18), 7664-7667.

15. Zhang, H.; Xu, X., Improving the transesterification and electrical conductivity of vitrimers by doping with conductive polymer wrapped carbon nanotubes. Composites Part A: Applied Science and Manufacturing 2017, 99, 15-22.

16. Denissen, W.; Rivero, G.; Nicolaÿ, R.; Leibler, L.; Winne, J. M.; Du Prez, F. E., Vinylogous Urethane Vitrimers. Advanced Functional Materials 2015, 25 (16), 2451-2457.

17. Tellers, J.; Pinalli, R.; Soliman, M.; Vachon, J.; Dalcanale, E., Reprocessable vinylogous urethane cross-linked polyethylene via reactive extrusion. Polymer Chemistry 2019, 10 (40), 5534-5542.

18. Hendriks, B.; Waelkens, J.; Winne, J. M.; Du Prez, F. E., Poly(thioether) Vitrimers via Transalkylation of Trialkylsulfonium Salts. ACS Macro Letters 2017, 6 (9), 930-934.

19. Obadia, M. M.; Mudraboyina, B. P.; Serghei, A.; Montarnal, D.; Drockenmuller, E., Reprocessing and Recycling of Highly Cross-Linked Ion-Conducting Networks through Transalkylation Exchanges of C–N Bonds. Journal of the American Chemical Society 2015, 137 (18), 6078-6083.

20. Azcune, I.; Odriozola, I., Aromatic disulfide crosslinks in polymer systems: Self-healing, reprocessability, recyclability and more. European Polymer Journal 2016, 84, 147-160.

21. Chen, M.; Zhou, L.; Wu, Y.; Zhao, X.; Zhang, Y., Rapid Stress Relaxation and Moderate Temperature of Malleability Enabled by the Synergy of Disulfide Metathesis and Carboxylate Transesterification in Epoxy Vitrimers. ACS Macro Letters 2019, 8 (3), 255-260.

22. Chao, A.; Negulescu, I.; Zhang, D., Dynamic Covalent Polymer Networks Based on Degenerative Imine Bond Exchange: Tuning the Malleability and Self-Healing Properties by Solvent.

Macromolecules 2016, 49 (17), 6277-6284.

23. Zhao, S.; Abu-Omar, M. M., Recyclable and Malleable Epoxy Thermoset Bearing Aromatic Imine Bonds. Macromolecules 2018, 51 (23), 9816-9824.

24. Zheng, J.; Png, Z. M.; Ng, S. H.; Tham, G. X.; Ye, E.; Goh, S. S.; Loh, X. J.; Li, Z., Vitrimers: Current research trends and their emerging applications. Materials Today 2021, 51, 586-625.

25. Fortman, D. J.; Brutman, J. P.; Cramer, C. J.; Hillmyer, M. A.; Dichtel, W. R., Mechanically Activated, Catalyst-Free Polyhydroxyurethane Vitrimers. Journal of the American Chemical Society 2015, 137 (44), 14019-14022.

26. Pepels, M.; Filot, I.; Klumperman, B.; Goossens, H., Self-healing systems based on disulfide–thiol exchange reactions. Polymer Chemistry 2013, 4 (18), 4955-4965.

27. Spiesschaert, Y.; Guerre, M.; De Baere, I.; Van Paepegem, W.; Winne, J. M.; Du Prez, F. E., Dynamic Curing Agents for Amine-Hardened Epoxy Vitrimers with Short (Re)processing Times. Macromolecules 2020, 53 (7), 2485-2495.

28. Ma, J.; Porath, L. E.; Haque, M. F.; Sett, S.; Rabbi, K. F.; Nam, S.; Miljkovic, N.; Evans, C. M., Ultra-thin self-healing vitrimer coatings for durable hydrophobicity. Nature Communications 2021, 12 (1), 5210.

29. Alabiso, W.; Schlögl, S. The Impact of Vitrimers on the Industry of the Future: Chemistry, Properties and Sustainable Forward-Looking Applications Polymers [Online], 2020.

30. Ruiz de Luzuriaga, A.; Martin, R.; Markaide, N.; Rekondo, A.; Cabañero, G.; Rodríguez, J.; Odriozola, I., Epoxy resin with exchangeable disulfide crosslinks to obtain reprocessable, repairable and recyclable fiber-reinforced thermoset composites. Materials Horizons 2016, 3 (3), 241-247.

31. Delahaye, M.; Winne, J. M.; Du Prez, F. E., Internal Catalysis in Covalent Adaptable Networks: Phthalate Monoester Transesterification As a Versatile Dynamic Cross-Linking Chemistry. Journal of the American Chemical Society 2019, 141 (38), 15277-15287.

32. Feng, X.; Li, G., Catalyst-free β-hydroxy phosphate ester exchange for robust fire-proof vitrimers. Chemical Engineering Journal 2021, 417, 129132.

33. Figueirêdo, M. B.; Heeres, H. J.; Deuss, P. J., Ozone mediated depolymerization and solvolysis of technical lignins under ambient conditions in ethanol. Sustainable Energy & Fuels 2020, 4 (1), 265-276.

34. Zhang, S.; Liu, T.; Hao, C.; Wang, L.; Han, J.; Liu, H.; Zhang, J., Preparation of a lignin-based vitrimer material and its potential use for recoverable adhesives. Green Chemistry 2018, 20 (13), 2995-3000.

35. Lucherelli, M. A.; Duval, A.; Avérous, L., Biobased vitrimers: Towards sustainable and adaptable performing polymer materials. Progress in Polymer Science 2022, 127, 101515.

36. Feng, X.; Li, G., Versatile Phosphate Diester-Based Flame Retardant Vitrimers via Catalyst-Free Mixed Transesterification. ACS Applied Materials & Interfaces 2020, 12 (51), 57486-57496.

37. Hubbard, A. M.; Ren, Y.; Papaioannou, P.; Sarvestani, A.; Picu, C. R.; Konkolewicz, D.; Roy, A. K.; Varshney, V.; Nepal, D., Vitrimer Composites: Understanding the Role of Filler in Vitrimer Applicability. ACS Applied Polymer Materials 2022, 4 (9), 6374-6385.

38. Riahi, A. M., Short-Term and Long-Term Mechanical Properties of CIPP Liners, Master's Thesis, University of Waterloo, Waterloo, ON, USA, 2015.

39. ASTM International. Standard Practice for Rehabilitation of Existing Pipelines and Conduits by the Inversion and Curing of a Resin-Impregnated Tube. 2009.

40. NASTT, CIPP Mechanical Properties and Testing, in Nastt's Cured-in-Place (CIPP) Good Practices Guidelines, North American Society for Trenchless Technology: Cleveland, OH, USA, pp. 2–17, 2015.

41. Ji, H. W.; Koo, D. D.; and Kang, J. H., Short- and Long-Term Structural Characterization of Cured-in-Place Pipe Liner with Reinforced Glass Fiber Material, Int. J. Environ. Res. Public Health, 17, 2073, 2020.

42. Ji, H. W.; Yoo, S. S.; Kim, J.; and Koo, D. D., The mechanical properties of high strength reinforced cured-in-place pipe (CIPP) liner composites for urban water infrastrcuture rehavilitation, Water, 10, 983, 2018.

43. Nassar, R.; Yousef, M., Analysis of creep failure times of cured-in-place pipe rehabilitation liners, Tunn. Undergr. Space Technol. 2002, 17, 327–332.

44. Lancaster, I.; and Zarghamee, M., The Evolution of Carbon Fiber CIPP (CFCIPP) for Small Diameter Potable Water & Fire Suppression Systems, In Proceedings of the North American Society for Trenchless Technology (NASTT), No Dig 2019 Conference, Chicago, IL, USA, 17–20 March 2019.

45. Dong, C.; Davies, I.J. Flexural properties of e glass and tr50s carbon fiber reinforced epoxy hybrid composites. J. Mater. Eng. Perform. 2013, 22, 41–49.

46. Shepherd, J., Carbon Fiber Calling: Carbon fiber-reinforced cured-in-place pipe renews fire suppression lines at energy facility, Pipeline Distribution, May 3 2019.

47. Jojibabu, P.; Jagannatham, M.; Haridoss, P.; Janaki Ram, G. D.; Deshpande, A. P.; Bakshi, S .R., Effect of different carbon nano-fillers on rheological properties and lap shear strength of epoxy adhesive joints. Compos Part A Appl Sci Manuf 2016;82:53–64. https://doi.org/10.1016/j.compositesa.2015.12.003.

48. Kausar, A.; Rafique, I.; and Muhammad, B., Review of Applications of Polymer /Carbon Nanotubes and Epoxy / CNT Composites, Polym.–Plast. Technol. Eng., 55, 1167-1191, 2016. https://doi.org/10.1080/03602559.2016.1163588.

49. Li, Y.; Wang, Q.; and Wang, S., A review on Enhancement of Mechanical and Tribological Properties of Polymer Composites Reinforced by Carbon Nanotubes and Graphene Sheet: Molecular Dynamics Simulations, Compos. Part B Eng., 160, 348-361, 2019. https://doi.org/10.1016/j.compositesb.2018.12.026.

50. Pandey, G.; and Thostenson, E. T., Carbon Nanotube-based Multifunctional Polymer Nanocomposites, Polym. Rev., 52, 355-3416, 2012.

51. Thess, A.; Lee, R.; Nikolaev, P.; Dai, H.; Petit, P.; and Robert, J., Crystalline Ropes of Metallic Carbon Nanotubes, Science 273, 483-487, 1996.

52. Gao, E.; Lu, W.; and Xu, Z., Strength Loss of Carbon Nanotube Fibers Explained in a Three-level Hierarchical Model, Carbon N Y, 138, 134-142, 2018.

53. Zhan, G. D.; Kuntz, J. D.; Garay, J. E.; and Mukherjee, A. K., Electrical Properties of Nanoceramics Reinforced with Ropes of Single-walled Carbon Nanotubes, Appl. Phys. Lett., 83, 1228-1230, 2003.

54. Pircheraghi, G.; Foudazi, R.; and Manas-Zloczower, I., Characterization of Carbon Nanotube Dispersion and Filler Network Formation in Melted Polyol for Nanocomposite Materials, Powder Technol., 276, 222-231, 2015.

55. Zhang, D.; and Huang, Y., Dispersion Characterizations and Adhesion Properties of Epoxy Composites Reinforced by Carboxymethyl Cellulose Surface Treated Carbon Nanotubes, Powder Technology, 404, 117505, May 2022.

56. Chia, L.; Huang, Y.; Bezbaruah, A.; and Lu, P., Carboxymethyl Cellulose Surface Treatment Method to Disperse Carbon Nanotubes in Smart Cementitious Materials, IEEE Sensor Journal, 21(13), pp.15218-15229, 2021.

57. Abd El-Lateef, H. M.; Sayed, A. R.; Gomha, S. M.; Bakir, E. M.; Shalabi, K., Synthesis and study of poly[(hydrazinylazo)]thiazoles as potent corrosion inhibitors for cast iron-carbon alloy in molar HCl: A collective computational and experiential methods. Journal of Molecular Liquids 2021, 337, 116555.

58. Suzudo, T.; Ebihara, K.; Tsuru, T., Brittle-fracture simulations of curved cleavage cracks in α-iron: A molecular dynamics study. AIP Advances 2020, 10 (11), 115209.

59. DeCelis, B.; Argon, A. S.; Yip, S., Molecular dynamics simulation of crack tip processes in alpha-iron and copper. Journal of Applied Physics 1983, 54 (9), 4864-4878.

60. Ma, L.; Xiao, S.; Deng, H.; Hu, W., Molecular dynamics simulation of fatigue crack propagation in bcc iron under cyclic loading. International Journal of Fatigue 2014, 68, 253-259.

61. Ambrish, S.; Kashif, R. A.; Mumtaz, A. Q.; Yuanhua, L., Investigation of Corrosion Inhibitors Adsorption on Metals Using Density Functional Theory and Molecular Dynamics Simulation, Corrosion Inhibitors, p Ch. 7, 2019.

62. Haris, N. I.; Sobri, S.; Yusof, Y. A.; Kassim, N. K., An Overview of Molecular Dynamic Simulation for Corrosion Inhibition of Ferrous Metals. Metals 2021, 11 (1).

63. Błoński, P.; Kiejna, A., Structural, electronic, and magnetic properties of bcc iron surfaces. Surface Science 2007, 601 (1), 123-133.

64. Yu, M.-F.; Lourie, O.; Dyer, M. J.; Moloni, K.; Kelly, T. F.; Ruoff, R. S., Strength and Breaking Mechanism of Multiwalled Carbon Nanotubes Under Tensile Load. Science 2000, 287 (5453), 637-640.

65. Montarnal, D.; Capelot, M.; Tournilhac, F.; Leibler, L., Silica-Like Malleable Materials from Permanent Organic Networks. Science 2011, 334 (6058), 965-968.

66. Deng, J.; Kuang, X.; Liu, R.; Ding, W.; Wang, A. C.; Lai, Y.-C.; Dong, K.; Wen, Z.; Wang, Y.; Wang, L.; Qi, H. J.; Zhang, T.; Wang, Z. L., Vitrimer Elastomer-Based Jigsaw Puzzle-Like Healable Triboelectric Nanogenerator for Self-Powered Wearable Electronics. Advanced Materials 2018, 30 (14), 1705918.

67. Hajj, R.; Duval, A.; Dhers, S.; Avérous, L., Network Design to Control Polyimine Vitrimer Properties: Physical Versus Chemical Approach. Macromolecules 2020, 53 (10), 3796-3805.

68. Wu, X.; Yang, X.; Yu, R.; Zhao, X.-J.; Zhang, Y.; Huang, W., A facile access to stiff epoxy vitrimers with excellent mechanical properties via siloxane equilibration. Journal of Materials Chemistry A 2018, 6 (22), 10184-10188.

69. Lu, Y.-X.; Guan, Z., Olefin Metathesis for Effective Polymer Healing via Dynamic Exchange of Strong Carbon–Carbon Double Bonds. Journal of the American Chemical Society 2012, 134 (34), 14226-14231.

70. Van Zee, N. J.; Nicolaÿ, R., Vitrimers: Permanently crosslinked polymers with dynamic network topology. Progress in Polymer Science 2020, 104, 101233.

71. Wang, S.; Urban, M. W., Self-healing polymers. Nature Reviews Materials 2020, 5 (8), 562-583.

72. Zheng, N.; Xu, Y.; Zhao, Q.; Xie, T., Dynamic Covalent Polymer Networks: A Molecular Platform for Designing Functions beyond Chemical Recycling and Self-Healing. Chemical Reviews 2021, 121 (3), 1716-1745.

73. Zhao, H.; Wei, X.; Fang, Y.; Gao, K.; Yue, T.; Zhang, L.; Ganesan, V.; Meng, F.; Liu, J., Molecular Dynamics Simulation of the Structural, Mechanical, and Reprocessing Properties of Vitrimers Based on a Dynamic Covalent Polymer Network. Macromolecules 2022, 55 (4), 1091-1103.

74. Yang, H.; Zheng, X.; Sun, Y.; Yu, K.; He, M.; Guo, Y., A molecular dynamics study on the surface welding and shape memory behaviors of Diels-Alder network. Computational Materials Science 2017, 139, 48-55.

75. Zheng, X.; Yang, H.; Sun, Y.; Zhang, Y.; Guo, Y., A molecular dynamics simulation on self-healing behavior based on disulfide bond exchange reactions. Polymer 2021, 212, 123111.

76. Sun, Y.; Yang, H.; Xia, W.; Guo, Y., Molecular dynamics simulations of surface welding in crosslinked networks with thermally reversible linkages. Applied Surface Science 2020, 527, 146947.

77. Sun, H., COMPASS: An ab Initio Force-Field Optimized for Condensed-Phase ApplicationsOverview with Details on Alkane and Benzene Compounds. The Journal of Physical Chemistry B 1998, 102 (38), 7338-7364.

78. Sun, H.; Ren, P.; Fried, J. R., The COMPASS force field: parameterization and validation for phosphazenes. Computational and Theoretical Polymer Science 1998, 8 (1), 229-246.

79. Tanemura, M.; Ogawa, T.; Ogita, N., A new algorithm for three-dimensional voronoi tessellation. Journal of Computational Physics 1983, 51 (2), 191-207.

80. Rigby, D.; Roe, R. J., Molecular dynamics simulation of polymer liquid and glass. 4. Free-volume distribution. Macromolecules 1990, 23 (26), 5312-5319.

81. Kresse, G.; Hafner, J., Ab initio molecular dynamics for liquid metals. Physical Review B 1993, 47 (1), 558-561.

82. Kresse, G.; Hafner, J., Ab initio molecular dynamics for open-shell transition metals. Physical Review B 1993, 48 (17), 13115-13118.

83. Qiao, Q.; Li, X.; Huang, L., Crystalline Cellulose under Pyrolysis Conditions: The Structure–Property Evolution via Reactive Molecular Dynamics Simulations. Journal of Chemical & Engineering Data 2020, 65 (2), 360-372.

84. Marashizadeh, P.; Abshirini, M.; Saha, M.; Huang, L.; Liu, Y., Atomistic Simulations on Structural Characteristics of ZnO Nanowire-Enhanced Graphene/Epoxy Polymer Composites: Implications for Lightweight Structures. ACS Applied Nano Materials 2021, 4 (11), 11770-11778.

85. Venable, R. M.; Krämer, A.; Pastor, R. W., Molecular Dynamics Simulations of Membrane Permeability. Chemical Reviews 2019, 119 (9), 5954-5997.

86. Kalra, A.; Hummer, G.; Garde, S., Methane Partitioning and Transport in Hydrated Carbon Nanotubes. The Journal of Physical Chemistry B 2004, 108 (2), 544-549.

87. Harris, J. G.; Yung, K. H., Carbon Dioxide's Liquid-Vapor Coexistence Curve And Critical Properties as Predicted by a Simple Molecular Model. The Journal of Physical Chemistry 1995, 99 (31), 12021-12024.

88. Thompson, A. P.; Aktulga, H. M.; Berger, R.; Bolintineanu, D. S.; Brown, W. M.; Crozier, P. S.; in 't Veld, P. J.; Kohlmeyer, A.; Moore, S. G.; Nguyen, T. D.; Shan, R.; Stevens, M. J.; Tranchida, J.; Trott, C.; Plimpton, S. J., LAMMPS - a flexible simulation tool for particle-based materials modeling at the atomic, meso, and continuum scales. Computer Physics Communications 2022, 271, 108171.

89. Kenyon Pipeline Inspection, CCTV Pipe Inspection - KPI Sewer, https://www.kpisewer.com/services/cctv-inspection/attachment/cctv-tn2/, accessed 01/03/2023

90. Hansen, C., New Standards for Testing and Certifying Cured-in-Place Pipe, Electro Scan Inc., 2017.

91. Electro Scan Inc., Focused Electrode Leak Location (FELL) Pipeline Assessment By Major Pipe Materials, 2019.

92. Jeff, G., Sensor System Records CIPP Temperature Readings During Installation, Underground Construction, November 2010, https://ucononline.com/magazine/2010/november-2010-vol-65-no-11/features/sensor-system-records-cipp-temperature-readings-during-installation

93. NASTT, Fiber Optic Cure Verification (FCV) Ensures Quality, Longevity of CIPP Liner Installations, in No-DIG show 2012, Paper C-6-05, March 2012.

94. USEPA, Report Field Demonstration of Condition Assessment Technologies, EPA_600 R-11 078, July 2011, Kathy Martel, P.E., The Cadmus Group, Inc., Chris Feeney, P.E., Louis Berger Group, Inc., Mary Ellen Tuccillo, Ph.D., The Cadmus Group, Inc., Contract No. EP-C-05-058, Task Order No. 59.

95. Yang, K.; Fang, H.; Zhang, X.; Li, B.; Hu, Q., Investigation of mechanical properties of corroded concrete pipes after cured-in-place-pipe (CIPP) rehabilitation under multi-field coupling. Tunnelling and Underground Space Technology 2022, 128, 104656.

96. Yang, K.; Xue, B.; Fang, H.; Du, X.; Li, B.; Chen, J., Mechanical sensitivity analysis of pipe-liner composite structure under multi-field coupling. Structures 2021, 29, 484-493.

97. Brown, M. J. P.; Moore, I. D.; Fam, A., Analysis of a cured-in-place pressure pipe liner spanning circular voids. Tunnelling and Underground Space Technology 2020, 101, 103424.

98. Brown, M. J. P.; Moore, I. D.; Fam, A., Performance of a cured-in-place pressure pipe liner passing through a pipe section without structural integrity. Tunnelling and Underground Space Technology 2014, 42, 87-95.

99. ASTM International, ASTM F 2207-06, Standard Specification for Cured-in-Place Pipe Lining System for Rehabilitation of Metallic Gas Pipe. ASTM International, West Conshohocken, PA, 2006.

100. Lu, H.; Wu, X.; Ni, H.; Azimi, M.; Yan, X.; Niu, Y., Stress analysis of urban gas pipeline repaired by inserted hose lining method. Composites Part B: Engineering 2020, 183, 107657.

101. Fang, H.; Yang, K.; Li, B.; He, H.; Xue, B., Parameter Analysis of Wall Thickness of Cured-in-Place Pipe Linings for Semistructured Rehabilitation of Concrete Drainage Pipe. Mathematical Problems in

Engineering 2020, 2020, 5271027.

102. Barsoum, I.; Dymock, J.; Walters, R.; Seibi, A., Finite-Element Analysis of the Installation Process of a Novel Corrosion Protective Kevlar-Reinforced Flexible Composite Liner. Journal of Pipeline Systems Engineering and Practice 2018, 9 (4), 04018022.

103. Shou, K. J.; Chen, B. C., Numerical analysis of the mechanical behaviors of pressurized underground pipelines rehabilitated by cured-in-place-pipe method. Tunnelling and Underground Space Technology 2018, 71, 544-554.

104. Li, Z.; Tang, Y.; Tang, F.; Chen, Y.; Chen, G., Elastic buckling of thin-walled polyhedral pipe liners encased in a circular pipe under uniform external pressure. Thin-Walled Structures 2018, 123, 214-221.

105. Rueda, F.; Marquez, A.; Otegui, J. L.; Frontini, P. M., Buckling collapse of HDPE liners: Experimental set-up and FEM simulations. Thin-Walled Structures 2016, 109, 103-112.

106. Kim, Y. T.; Haghpanah, B.; Ghosh, R; Ali, H.; Hamouda, A. M. S.; and Vaziri, A., "Instability of a cracked cylindrical shell reinforced by an elastic liner," *Thin-walled structures,* vol. 70, pp. 39–48, 2013.

107. Li, Z.; Wang, L.; Guo, Z.; Shu, H., Elastic buckling of cylindrical pipe linings with variable thickness encased in rigid host pipes. Thin-Walled Structures 2012, 51, 10-19.

108. Rueda, F.; Otegui, J. L.; Frontini, P., Numerical tool to model collapse of polymeric liners in pipelines. Engineering Failure Analysis 2012, 20, 25-34.

109. Chuk, C.; Urgessa, G.; Thippeswamy, H., Numerical analysis of stresses for cured-in-place-pipe linings, WIT Transactions on The Built Environment, 71, pp 283-293, 2011.

110. Zhao, Y.; Ma, B.; Ariaratnam, S. T.; Zeng, C.; Yan, X.; Wang, F.; Wang, T.; Zhu, Z.; He, C.; Shi, G.; Mi, R., Structural performance of damaged rigid pipe rehabilitated by centrifugal spray on mortar liner. Tunnelling and Underground Space Technology 2021, 116, 104117.

111. Patel, H.; Salehi, S., Structural integrity of liner cement in oil & gas wells: Parametric study, sensitivity analysis, and risk assessment. Engineering Failure Analysis 2021, 122, 105203.

112. Farrag, K.; "Evaluation of Structural Liners for the Rehabilitation of Liquid and Natural Gas Piping Systems," 2015.

113. El-Sawy, K.; Moore Ian, D., Parametric Study for Buckling of Liners: Effect of Liner Geometry and Imperfections. Trenchless Pipeline Projects, 416-423.

114. El-Sawy, K.; Moore Ian, D., Stability of Loosely Fitted Liners Used to Rehabilitate Rigid Pipes. Journal of Structural Engineering 1998, 124 (11), 1350-1357.

115. ASME International, ASME B31.8S-2018 Managing System Integrity of Gas Pipelines, ASME Code for Pressure Piping, B31 Supplement to ASME B31.8, New York, NY, 2018.

116. Raeihagh, H.; Behbahaninia, A.; Macki Aleagha, M., Risk assessment of sour gas inter-phase onshore pipeline using ANN and fuzzy inference system – Case study: The south pars gas field. Journal of Loss Prevention in the Process Industries 2020, 68, 104238.

117. Zhang, L.; Wu, X.; Skibniewski, M. J.; Zhong, J.; Lu, Y., Bayesian-network-based safety risk analysis in construction projects. Reliability Engineering & System Safety 2014, 131, 29-39.

118. Guo, X.; Zhang, L.; Liang, W.; Haugen, S., Risk identification of third-party damage on oil and gas pipelines through the Bayesian network. Journal of Loss Prevention in the Process Industries 2018, 54, 163-178.

119. Hasan, S.; Khan, F.; Kenny, S., Probability assessment of burst limit state due to internal corrosion. International Journal of Pressure Vessels and Piping 2012, 89, 48-58.

120. Qiu, Q.; Cui, L., Reliability evaluation based on a dependent two-stage failure process with competing failures. Applied Mathematical Modelling 2018, 64, 699-712.

121. Shabarchin, O.; Tesfamariam, S., Internal corrosion hazard assessment of oil & gas pipelines using Bayesian belief network model. Journal of Loss Prevention in the Process Industries 2016, 40, 479-495.

122. Bai, M.; Du, Y.; Chen, Y.; Xing, Y.; Zhao, P., Risk Assessment of Long Gas and Oil Pipeline Projects Inducing Landslide Disasters during Construction. Journal of Performance of Constructed Facilities 2017, 31 (5), 04017063.

123. Kabir, G.; Sadiq, R.; Tesfamariam, S., A fuzzy Bayesian belief network for safety assessment of oil and gas pipelines. Structure and Infrastructure Engineering 2016, 12 (8), 874-889.

124. Yajima, A.; Wang, H.; Liang, R. Y.; Castaneda, H., A clustering based method to evaluate soil corrosivity for pipeline external integrity management. International Journal of Pressure Vessels and Piping 2015, 126-127, 37-47.

125. Senouci, A.; Elabbasy, M.; Elwakil, E.; Abdrabou, B.; Zayed, T., A model for predicting failure of oil pipelines. Structure and Infrastructure Engineering 2014, 10 (3), 375-387.

126. Dawood, T.; Elwakil, E.; Novoa, H. M.; Delgado, J. F. G., 3D Modeling of Pipe Risk Index for a Sustainable Urban Water System. 2021 IEEE Conference on Technologies for Sustainability (SusTech) 2021, 1-6.

127. Dawood, T.; Elwakil, E.; Mayol Novoa, H.; Fernando Gárate Delgado, J., Pressure data-driven model for failure prediction of PVC pipelines. Engineering Failure Analysis 2020, 116, 104769.

128. Chae Myung, J.; Abraham Dulcy, M., Neuro-Fuzzy Approaches for Sanitary Sewer Pipeline Condition Assessment. Journal of Computing in Civil Engineering 2001, 15 (1), 4-14.

129. Li, X.; Chen, G.; Zhu, H., Quantitative risk analysis on leakage failure of submarine oil and gas pipelines using Bayesian network. Process Safety and Environmental Protection 2016, 103, 163-173.

130. Chen, S. Y.; Lin, M. S.; Hsiao, G. L.; Wang, T. C.; Kao, C. S., Underground Pipeline Leakage Risk Assessment in an Urban City. Int J Environ Res Public Health 2020, 17 (11), E3929.

131. Liu, Y.; Ma, X.; Li, Y.; Tie, Y.; Zhang, Y.; Gao, J., Water Pipeline Leakage Detection Based on Machine Learning and Wireless Sensor Networks. Sensors 2019, 19 (23).

132. Shin, H.; Joo, C.; Koo, J., Optimal Rehabilitation Model for Water Pipeline Systems with Genetic Algorithm. Procedia Engineering 2016, 154, 384-390.

133. Khalid, H. U.; Ismail, M. C.; Nosbi, N., Permeation Damage of Polymer Liner in Oil and Gas Pipelines: A Review. Polymers 2020, 12 (10).

134. Kiefner, J. F.; Trench, C. J. Oil Pipeline Characteristics and Risk Factors: Illustrations from the Decade of Construction; 2001.